Near-Field Integrated Sensing and Communication: SPEB Analysis and Hybrid Beamforming Design

Minghao Yuan, Dongxuan He, *Member, IEEE*, Weijie Yuan, *Senior Member, IEEE*, Hao Yin, and Hua Wang, *Member, IEEE*

***Abstract*— This paper investigates hybrid beamforming (HBF) design for near-field millimeter wave (mmWave) integrated sensing and communication (ISAC) systems, where one base station (BS) equipped with large-scale antenna array simultaneously serves multiple communication users and performs target localization by exploiting the degrees of freedom in both angle and distance domains. First, to characterize the target localization accuracy, we analyze the squared position error bound (SPEB) for estimating the two-dimensional (2D) position of target. Then, two HBF optimization problems are formulated to investigate the tradeoff between localization accuracy and communication rate. For the sensing-oriented optimization, we aim to minimize the SPEB of target localization while ensuring the communication rate requirements of individual users. To tackle this nonconvex problem, we propose a semidefinite relaxation (SDR)-based block coordinate descent (BCD) algorithm. For the communication-oriented optimization, a fractional programming (FP) and successive convex approximation (SCA)-based BCD algorithm is proposed to solve the sum-rate maximization problem under the SPEB constraint. The convergence and complexity analyses of the proposed algorithms are presented. Simulation results demonstrate that the proposed HBF algorithms can achieve localization accuracy and communication rate close to fully-digital beamforming and outperform the benchmark schemes.**

***Index Terms*— Integrated sensing and communication, near-field, target localization, squared position error bound, hybrid beamforming.**

I. Introduction

NEXT-GENERATION wireless networks are expected to possess both high-capacity communication and high-accuracy sensing abilities for empowering many emerging applications, such as extended reality, intelligent transportation, and low-altitude economy [1], [2]. Integrated sensing and communication (ISAC) is envisioned to simultaneously achieve both sensing and communication functionalities by sharing spectrum, hardware, and waveform, thus improving resource utilization efficiency and realizing mutual benefits [1], [3]. Recently, ISAC has been widely recognized as one of the most potential technologies for the sixth-generation (6G) wireless networks [4], [5]. To meet the increasingly growing demand for communication and sensing performance, wireless communication systems are evolving towards extremely large-scale antenna arrays and high frequency bands, such as millimeter wave (mmWave) and Terahertz (THz), thereby providing possibilities for achieving high-capacity communication and high-accuracy sensing [6].

However, the increased array aperture and carrier frequency lead to the paradigm shift of electromagnetic characteristics, i.e., from the planar-wave-based far-field propagation to the spherical-wave-based near-field propagation [7], [8], [9], [10]. In the near-field channel, the conventional system designs based on the far-field assumption suffer from significant performance degradation, thus necessitating tailored near-field technologies [7], [8], [9]. Meanwhile, the transformation of electromagnetic characteristics provides new opportunities for the system design of both communication and sensing [10], [11], [12]. From the perspective of communication, compared to the far-field channel, the near-field channel introduces an additional degree of freedom in the distance domain. Leveraging both the angle and distance information incorporated in the spherical-wave model, near-field communication can concentrate beam energy on the specific locations, thus achieving high-resolution beamfocusing and efficient interference management [10]. On the other hand, the near-field channel can offer larger spatial multiplexing gain and communication capacity than the far-field channel. From the perspective of sensing, the spherical wavefront can be exploited to achieve target localization through the joint estimation of angle and distance [11], [12].

A. Related Works

1) Near-Field Communication: In recent years, the potential of near-field communication has been widely explored in terms of channel estimation [13], beam training [14], and beamforming [15]. In [13], exploiting the polar-domain sparsity of the near-field channel, two compressive sensing (CS)-based channel estimation algorithms were proposed

Received 30 March 2025; revised 18 July 2025; accepted 18 August 2025. Date of publication 26 August 2025; date of current version 31 December 2025. This work was supported in part by the National Key Research and Development Program of China under Grant 2024YFE0200404 and Grant 2020YFB1807900; and in part by the National Natural Science Foundation of China under Grant 62101306. The associate editor coordinating the review of this article and approving it for publication was X. Mu. *(Corresponding author: Dongxuan He.)*

Minghao Yuan, Dongxuan He, and Hua Wang are with the School of Information and Electronics, Beijing Institute of Technology, Beijing 100081, China (e-mail: minghaoyuan@bit.edu.cn; dongxuan_he@bit.edu.cn; wanghua@bit.edu.cn).

Weijie Yuan is with the School of Automation and Intelligent Manufacturing, Southern University of Science and Technology, Shenzhen 518055, China (e-mail: yuanwj@sustech.edu.cn).

Hao Yin is with Beijing Institute of Electronic System Engineering, Beijing 100141, China (e-mail: yinhao@cashq.ac.cn).

Digital Object Identifier 10.1109/TCCN.2025.3602802

for extremely large-scale multiple-input multiple-output (XL-MIMO) to achieve improved estimation accuracy compared to existing far-field channel estimation techniques. In addition, a near-field hierarchical beam training method based on multi-resolution codebooks was proposed to reduce the training overhead [14]. For downlink multiuser MIMO systems, the potential of near-field beamfocusing in mitigating interuser interference and improving achievable sum-rate was demonstrated in [15].

2) Near-Field Sensing and Localization: Near-field spherical-wave propagation characteristic facilitates the joint estimation of angle and distance, making it possible to realize target localization through only single node and limited bandwidth. Recently, performance bound analysis [16], [17] and target parameter estimation [17] for near-field sensing and localization have received considerable interest. Typically, the Cramér-Rao bound (CRB) is adopted to evaluate parameter estimation performance and facilitate waveform and beamforming optimization. Specifically, in [16], the closed-form near-field CRB expressions for angle and range estimation were derived for XL-MIMO radar and XL-phased array radar, respectively. Instead of polar coordinate system [16], the position of target was characterized in Cartesian coordinate system [17]. The authors in [17] analyzed the near-field CRB for estimating the three-dimensional (3D) coordinates of target and proposed two localization algorithms based on the maximum likelihood (ML) criterion.

3) Near-Field ISAC: Recently, the research on near-field ISAC has attracted increasing attention [11], [12], [18], [19], [20]. In [18], beamforming design for multiuser near-field ISAC systems was investigated to minimize the CRB for joint distance and angle sensing while satisfying the communication rate requirement of each user. Moreover, the authors in [19] analyzed the performance degradation in communication and sensing caused by far-field beamforming in near-field channels. However, the aforementioned works [18], [19] consider fully-digital beamforming (FDBF) [21] or fully-connected hybrid beamforming (HBF) [22], [23], which inevitably lead to prohibitive hardware cost and energy consumption, especially when large-scale antenna arrays are deployed. To reduce the hardware complexity, a partially-connected HBF design based on the penalty dual decomposition (PDD) method was proposed to minimize the joint angle and distance CRB for near-field ISAC systems [20]. Nevertheless, the PDD technique suffers from high computational complexity due to its double-loop structure [24].

B. Motivation and Contributions

Despite the extensive research progress, the prior works regarding near-field performance bound analysis [16] and beamforming design [18], [20] mainly focus on the CRB for joint distance and angle estimation, i.e., the sum of the CRB of distance estimation and the CRB of angle estimation. However, the measurement units of distance and angle are inconsistent, where the distance is measured in meters, and the angle is measured in degrees. Consequently, minimizing the CRB for joint distance and angle estimation cannot theoretically guarantee the target localization error minimization. Different from using the CRB to evaluate the performance of distance and angle estimation in the prior works [18], [20], we exploit the squared position error bound (SPEB) to intuitively characterize the accuracy of position estimation in this paper. The SPEB is defined as the trace of the inverse of the equivalent Fisher information matrix (EFIM) of the position parameters, which can provide a lower bound on the variance of any unbiased position estimator. In [25] and [26], the concept of SPEB was first proposed to develop a general framework to characterize the fundamental limit of localization accuracy of wireless networks. In recent years, the SPEB was widely adopted to analyze the localization accuracy limit [27], [28] and formulate the beamforming design [29], [30], [31], [32]. However, the above works [27], [28], [29], [30], [31], [32] only focus on far-field channels. To the best of our knowledge, near-field SPEB analysis and SPEB-based beamforming design have been not investigated yet. On the other hand, the aforementioned near-field ISAC beamforming designs [18], [19], [20] mainly concentrate on the sensing-oriented optimization [32], i.e., the sensing performance optimization under communication performance constraint. Nevertheless, the communication-oriented optimization in near-field channels is rarely studied. Motivated by the above issues, we aim to analyze the SPEB of near-field target localization and investigate the near-field ISAC beamforming design to explore the performance tradeoff between localization and communication.

In this paper, we investigate HBF design for near-field mmWave ISAC systems. The main contributions of this paper are summarized as follows:

- We propose a near-field mmWave ISAC system, where one base station (BS) equipped with large-scale antenna array simultaneously serves multiple communication users (CUs) and carries out target localization by exploiting the degrees of freedom in both angle and distance domains. To characterize the accuracy of near-field target localization, we derive the SPEB for estimating the two-dimensional (2D) Cartesian coordinates of target. Based on this, two HBF optimization problems are formulated to investigate the tradeoff between localization accuracy and communication rate.
- For the sensing-oriented optimization, our objective is to jointly design the analog beamformer and digital beamformer to minimize the SPEB of target localization, while guaranteeing the communication rate requirement of each CU, transmit power budget, and constant modulus constraints. The above nonconvex problem is first reformulated as a tractable form by leveraging the Schur complement. Then, we propose a semidefinite relaxation (SDR)-based block coordinate descent (BCD) algorithm to address the resulting problem.
- For the communication-oriented optimization, the HBF design is formulated to maximize the communication sum-rate subject to the target localization accuracy constraint, transmit power constraint, and constant modulus constraints. First, the intractable problem is equivalently

reformulated as an easy-to-handle one by exploiting the fractional programming (FP) method. Then, a successive convex approximation (SCA)-based BCD algorithm is proposed to tackle the problem.

- The convergence and complexity analyses of the proposed algorithms are presented. Simulation results show that the proposed sensing-oriented HBF design can achieve localization accuracy close to the corresponding FDBF and outperform the benchmark schemes, and the proposed communication-oriented HBF design can realize sum-rate similar to the FDBF counterpart and significantly surpass the existing methods.

The remainder of this paper is organized as follows. Section II introduces the near-field channel model and signal model. Section III analyzes the SPEB of near-field target localization and formulates two HBF optimization problems. Section IV proposes an SDR-based BCD algorithm to solve the communication rate-constrained SPEB minimization problem. Section V proposes an SCA-based BCD algorithm to tackle the SPEB-constrained communication sum-rate maximization problem. Simulation results are presented in Section VI. Finally, this paper is concluded in Section VII.

Notations: Scalars, vectors, and matrices are denoted by the lowercase letters, boldface lowercase letters, and boldface uppercase letters, respectively. $\mathbb{C}^{M\times N}$ and $\mathbb{R}^{M\times N}$ denote the spaces of $M\times N$ complex and real matrices, respectively. $(\cdot)^*$, $(\cdot)^T$, and $(\cdot)^H$ denote the conjugate, transpose, and conjugate transpose, respectively. $(\cdot)^{-1}$, $\|\cdot\|_F$, $\mathrm{tr}(\cdot)$, and $\mathrm{rank}(\cdot)$ denote the inversion, Frobenius norm, trace, and rank of a matrix, respectively. $[\mathbf{x}]_j$ denotes the j-th element of vector $\mathbf{x}$. $[\mathbf{X}]_{i,j}$ denotes the (i,j)-th element of matrix $\mathbf{X}$. $\mathrm{diag}\,()$ and $\mathrm{blkdiag}\,\{\}$ denote the operations of diagonalization and block diagonalization, respectively. $\mathbf{I}_N$ denotes an $N\times N$ identity matrix. $\mathbf{x}\sim\mathcal{CN}(\boldsymbol{\mu},\boldsymbol{\Sigma})$ denotes the complex Gaussian distribution with mean $\boldsymbol{\mu}$ and covariance matrix $\boldsymbol{\Sigma}$. $\mathbb{E}\{\cdot\}$ denotes the statistical expectation. $|\cdot|$ denotes the magnitude of a complex number. $||\cdot||$ denotes the 2-norm of a vector. $\mathrm{Re}\{\cdot\}$ and $\mathrm{Im}\{\cdot\}$ denote the real and imaginary parts of a complex number, respectively. The major notations used in the paper are listed in Table I.

TABLE I
LIST OF NOTATIONS

Notation	Definition
$\mathbf{p}_n^{\mathrm{BS}}=[x_n^{\mathrm{BS}},y_n^{\mathrm{BS}}]^T$	Position of the n-th antenna at the BS
$\mathbf{p}_k^{\mathrm{CU}}=[x_k,y_k]^T$	Position of the k-th CU
$\mathbf{p}^{\mathrm{ST}}=[x,y]^T$	Position of sensing target
$\mathbf{h}_k$	Communication channel of the k-th CU
$\mathbf{G}$	Sensing channel
$\mathbf{F}_{\mathrm{A}}$	Analog beamformer
$\mathbf{F}_{\mathrm{D}}$	Digital beamformer
$\mathbf{s}(t)$	Transmitted signal
$y_{\mathrm{c},k}(t)$	Received communication signal
$\mathbf{y}_{\mathrm{s}}(t)$	Received sensing echo signal
$\alpha_k^{\mathrm{LoS}},\alpha_{k,l}^{\mathrm{NLoS}}$	Channel amplitude of LoS path and NLoS path
β	Target reflection coefficient
$\mathbf{a}\,(x,y)$	Near-field array response vector

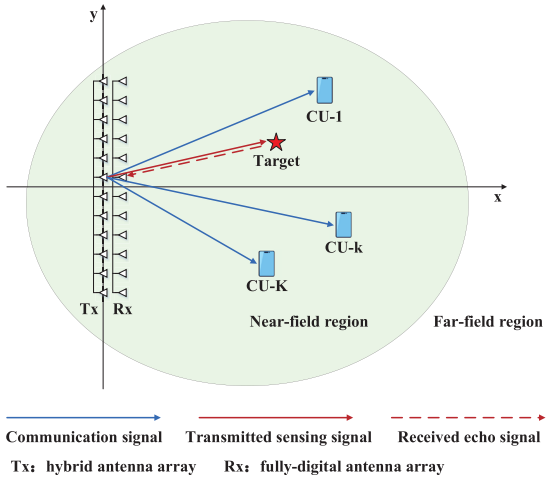

Fig. 1. System model.

II. System Model

As shown in Fig. 1, we consider a near-field mmWave ISAC system, where the BS consisting of the ISAC transmitter (Tx) equipped with N antennas and the sensing receiver (Rx) equipped with N antennas simultaneously serves K single-antenna CUs and carries out target localization. We assume that the BS is operated in monostatic sensing mode and is capable of achieving perfect self-interference cancellation [18], [20]. Without loss of generality, we assume that the Tx/Rx are equipped with uniform linear arrays (ULAs) with the antenna spacing of d, resulting in the array aperture of $D=(N-1)\,d$. Therefore, the Rayleigh distance is equal to $\frac{2D^2}{\lambda}$, where λ is the signal wavelength. It is assumed that both the CUs and sensing target are located in the near-field region of the BS. Let $\mathbf{p}_n^{\mathrm{BS}}=[x_n^{\mathrm{BS}},y_n^{\mathrm{BS}}]^T, n=1,\ldots,N$ denote the position of the n-th antenna of the Tx/Rx, $\mathbf{p}_k^{\mathrm{CU}}=[x_k,y_k]^T, k=1,\ldots,K$ denote the position of the k-th CU, and $\mathbf{p}^{\mathrm{ST}}=[x,y]^T$ denote the position of the sensing target.

To reduce the hardware cost and energy consumption, partially-connected HBF is adopted at the Tx [33], [34], [35]. Specifically, the Tx is equipped with N_{RF} RF chains, each of which is connected to a subarray with $M=N/N_{\mathrm{RF}}$ antennas through phase shifters. With the partially-connected architecture, the analog beamformer of the Tx can be represented as

$$\mathbf{F}_{\mathrm{A}}=\mathrm{blkdiag}\,\{\mathbf{f}_1,\ldots,\mathbf{f}_{N_{\mathrm{RF}}}\}, \tag{1}$$

where $\mathbf{f}_i\in\mathbb{C}^{M\times 1}$ represents the analog beamforming vector corresponding to the i-th subarray with each element satisfying the constant modulus constraint, i.e., $|\,[\mathbf{f}_i]_j\,|=1, i=1,\ldots,N_{\mathrm{RF}}, j=1,\ldots,M$.

A. Near-Field Channel Model

1) Near-Field Communication Channel Model: Without loss of generality, we assume that the center of the Tx/Rx

arrays is located at the origin of the coordinate system, i.e., $[0,0]^T$. The position of the n-th antenna of the Tx/Rx can be denoted by $\mathbf{p}_n^{\mathrm{BS}} = [0, \delta_n d]^T$, where $\delta_n = \frac{2n-N-1}{2}, n = 1, \ldots, N$ [6], [13]. Therefore, the distance from the n-th antenna of the Tx/Rx to the k-th CU can be calculated as

$$||\mathbf{p}_k^{\mathrm{CU}} - \mathbf{p}_n^{\mathrm{BS}}|| = \sqrt{x_k^2 + y_k^2 - 2\delta_n d y_k + \delta_n^2 d^2}. \quad (2)$$

Thus, the line-of-sight (LoS) near-field channel between the n-th antenna of the Tx and the k-th CU can be expressed as

$$h_{k,n}^{\mathrm{LoS}} = \alpha_{k,n}^{\mathrm{LoS}} e^{-j\frac{2\pi}{\lambda}||\mathbf{p}_k^{\mathrm{CU}} - \mathbf{p}_n^{\mathrm{BS}}||}, \quad (3)$$

where $\alpha_{k,n}^{\mathrm{LoS}}$ represents the distance-dependent channel amplitude between the n-th antenna and the k-th CU. Within the Fresnel region of the near-field, we assume that the channel amplitudes between all the antennas at the Tx and the k-th CU are approximately the same, i.e., $\alpha_{k,n}^{\mathrm{LoS}} = \alpha_k^{\mathrm{LoS}} = \frac{\lambda}{4\pi||\mathbf{p}_k^{\mathrm{CU}}||}, \forall n$ [18], [20]. Thus, the LoS near-field channel between the Tx and the k-th CU can be expressed as

$$\mathbf{h}_k^{\mathrm{LoS}} = \alpha_k^{\mathrm{LoS}} \mathbf{a}\left(x_k, y_k\right), \quad (4)$$

where α_k^{LoS} represents the channel amplitude of the LoS path, and $\mathbf{a}\left(x_k, y_k\right)$ represents the near-field array response vector of the LoS path, given by

$$\mathbf{a}\left(x_k, y_k\right) = \left[e^{-j\frac{2\pi}{\lambda}||\mathbf{p}_k^{\mathrm{CU}} - \mathbf{p}_1^{\mathrm{BS}}||}, \ldots, e^{-j\frac{2\pi}{\lambda}||\mathbf{p}_k^{\mathrm{CU}} - \mathbf{p}_N^{\mathrm{BS}}||}\right]^T. \quad (5)$$

The Saleh-Valenzuela model [6], [18], [20] is adopted to characterize the sparse scattering property of mmWave channels. For the k-th CU, the mmWave channel consisting of one LoS path and L_k non-line-of-sight (NLoS) paths can be expressed as

$$\mathbf{h}_k = \alpha_k^{\mathrm{LoS}} \mathbf{a}\left(x_k, y_k\right) + \sum_{l=1}^{L_k} \alpha_{k,l}^{\mathrm{NLoS}} \mathbf{a}\left(x_{k,l}, y_{k,l}\right), \quad (6)$$

where $\alpha_{k,l}^{\mathrm{NLoS}}$ represents the channel amplitude of the l-th NLoS path, and $\mathbf{a}\left(x_{k,l}, y_{k,l}\right)$ represents the near-field array response vector corresponding to the l-th scatterer associated with the k-th CU. It is assumed that accurate channel information can be efficiently acquired by adopting the advanced channel estimation technique [13].

2) Near-Field Sensing Channel Model: The distance between the n-th antenna of the Tx/Rx and the sensing target can be calculated as

$$||\mathbf{p}^{\mathrm{ST}} - \mathbf{p}_n^{\mathrm{BS}}|| = \sqrt{x^2 + y^2 - 2\delta_n d y + \delta_n^2 d^2}. \quad (7)$$

In mmWave bands, the signal attenuation of the NLoS path is much greater than that of the LoS paths, especially for target sensing. Therefore, we only consider the LoS path in target sensing [18], [19], [20]. The near-field sensing channel can be expressed as

$$\mathbf{G} = \beta \mathbf{a}\left(x, y\right) \mathbf{a}^H\left(x, y\right), \quad (8)$$

where β denotes the reflection coefficient including both the distance-dependent path loss and the radar cross section (RCS) of the target, and $\mathbf{a}\left(x, y\right)$ represents the near-field array response vector, given by

$$\mathbf{a}\left(x, y\right) = \left[e^{-j\frac{2\pi}{\lambda}||\mathbf{p}^{\mathrm{ST}} - \mathbf{p}_1^{\mathrm{BS}}||}, \ldots, e^{-j\frac{2\pi}{\lambda}||\mathbf{p}^{\mathrm{ST}} - \mathbf{p}_N^{\mathrm{BS}}||}\right]^T. \quad (9)$$

The target parameters can be obtained by employing the classical parameter estimation algorithms, such as multiple signal classification (MUSIC).

B. Near-Field Signal Model

1) Near-Field Communication Signal Model: For downlink multiuser communication, the signal transmitted by the Tx at the time instant t can be expressed as

$$\mathbf{x}(t) = \mathbf{F}_{\mathrm{A}} \mathbf{F}_{\mathrm{D}} \mathbf{s}(t) = \mathbf{F}_{\mathrm{A}} \sum_{k=1}^{K} \mathbf{f}_{\mathrm{D},k} s_k(t), \quad (10)$$

where $\mathbf{s}(t) = [s_1(t), \ldots, s_K(t)] \in \mathbb{C}^{K\times 1}$ represents the independent and identically distributed transmitted data symbol such that $\mathbb{E}\{\mathbf{s}(t)\mathbf{s}^H(t)\} = \mathbf{I}_K$, $\mathbf{F}_{\mathrm{D}} = [\mathbf{f}_{\mathrm{D},1}, \ldots, \mathbf{f}_{\mathrm{D},K}] \in \mathbb{C}^{N_{\mathrm{RF}}\times K}$ represents the digital beamformer, and $\mathbf{F}_{\mathrm{A}} \in \mathbb{C}^{N\times N_{\mathrm{RF}}}$ represents the analog beamformer.

The received signal of the k-th CU can be expressed as

$$y_{\mathrm{c},k}(t) = \mathbf{h}_k^H \mathbf{F}_{\mathrm{A}} \mathbf{f}_{\mathrm{D},k} s_k(t) + \sum_{j=1, j\neq k}^{K} \mathbf{h}_k^H \mathbf{F}_{\mathrm{A}} \mathbf{f}_{\mathrm{D},j} s_j(t) + z_{\mathrm{c},k}(t), \quad (11)$$

where $z_{\mathrm{c},k}(t)$ represents the Gaussian noise following $\mathcal{CN}(0, \sigma^2)$.

The signal-to-interference-plus-noise ratio (SINR) of the k-th CU can be represented as

$$\mathrm{SINR}_k = \frac{\left|\mathbf{h}_k^H \mathbf{F}_{\mathrm{A}} \mathbf{f}_{\mathrm{D},k}\right|^2}{\sum_{j=1, j\neq k}^{K} \left|\mathbf{h}_k^H \mathbf{F}_{\mathrm{A}} \mathbf{f}_{\mathrm{D},j}\right|^2 + \sigma^2}. \quad (12)$$

The achievable communication rate of the k-th CU can be represented as

$$R_k = \log\left(1 + \mathrm{SINR}_k\right). \quad (13)$$

2) Near-Field Sensing Signal Model: For target sensing, the echo signal received by the Rx at the t-th snapshot can be expressed as

$$\begin{aligned} \mathbf{y}_{\mathrm{s}}(t) &= \mathbf{G}\mathbf{x}(t) + \mathbf{z}_{\mathrm{s}}(t) \\ &= \beta \mathbf{a}\left(x, y\right) \mathbf{a}^H\left(x, y\right) \mathbf{x}(t) + \mathbf{z}_{\mathrm{s}}(t), \end{aligned} \quad (14)$$

where $\mathbf{z}_{\mathrm{s}}(t) \in \mathbb{C}^{N\times 1}$ denotes the Gaussian noise obeying $\mathcal{CN}(0, \sigma^2 \mathbf{I}_N)$. The received echo signal over T snapshots can be represented as

$$\mathbf{Y}_{\mathrm{s}} = \beta \mathbf{a}\left(x, y\right) \mathbf{a}^H\left(x, y\right) \mathbf{X} + \mathbf{Z}_{\mathrm{s}}, \quad (15)$$

where $\mathbf{Y}_{\mathrm{s}} = [\mathbf{y}_{\mathrm{s}}(1), \ldots, \mathbf{y}_{\mathrm{s}}(T)]$, $\mathbf{X} = [\mathbf{x}(1), \ldots, \mathbf{x}(T)]$, and $\mathbf{Z}_{\mathrm{s}} = [\mathbf{z}_{\mathrm{s}}(1), \ldots, \mathbf{z}_{\mathrm{s}}(T)]$. Let $\mathbf{S} = [\mathbf{s}(1), \ldots, \mathbf{s}(T)]$ denote the transmitted symbol over T snapshots. Thus, the transmit covariance matrix can be represented as

$$\begin{aligned} \mathbf{R}_{\mathrm{X}} = \frac{1}{T}\mathbf{X}\mathbf{X}^H &= \frac{1}{T}\mathbf{F}_{\mathrm{A}}\mathbf{F}_{\mathrm{D}}\mathbf{S}\mathbf{S}^H\mathbf{F}_{\mathrm{D}}^H\mathbf{F}_{\mathrm{A}}^H \\ &\approx \mathbf{F}_{\mathrm{A}}\mathbf{F}_{\mathrm{D}}\mathbf{F}_{\mathrm{D}}^H\mathbf{F}_{\mathrm{A}}^H. \end{aligned} \quad (16)$$

Notice that this approximation in (16) can be regarded as an accurate equality when T is sufficiently large [21].

III. SPEB Analysis and Problem Formulation

A. SPEB Analysis

The fundamental limit of localization accuracy is typically characterized by the SPEB [25], [26], [27], [28]. Different from using the CRB to evaluate the performance of distance and angle estimation in the prior works [18], [20], we utilize the SPEB to directly characterize the near-field target localization accuracy in this paper.

To facilitate the SPEB analysis, the received echo signal in (15) is vectorized as

$$\tilde{\mathbf{y}}_{\mathrm{s}} = \mathrm{vec}\left(\mathbf{Y}_{\mathrm{s}}\right) = \boldsymbol{\eta} + \tilde{\mathbf{z}}_{\mathrm{s}}, \tag{17}$$

where $\boldsymbol{\eta} = \beta \mathrm{vec}\left(\mathbf{a}\left(x,y\right)\mathbf{a}^{H}\left(x,y\right)\mathbf{X}\right) \in \mathbb{C}^{NT\times 1}$, and $\tilde{\mathbf{z}}_{\mathrm{s}} = \mathrm{vec}\left(\mathbf{Z}_{\mathrm{s}}\right)$ follows the Gaussian distribution $\mathcal{CN}(0,\sigma^2\mathbf{I}_{NT})$. Let $\boldsymbol{\xi} = [\mathbf{p}^{\mathrm{ST}}, \tilde{\boldsymbol{\beta}}]^T \in \mathbb{R}^{4\times 1}$ denote the vector of unknown parameters, where $\mathbf{p}^{\mathrm{ST}} = [x,y]^T$ is the target position parameter of interest, $\tilde{\boldsymbol{\beta}} = \left[\mathrm{Re}\left\{\beta\right\}, \mathrm{Im}\left\{\beta\right\}\right]^T$ is the nuisance parameter [28]. For notational convenience, let $\mathbf{A} = \mathbf{a}\left(x,y\right)\mathbf{a}^{H}\left(x,y\right)$.

Then, we derive the Fisher information matrix (FIM) for estimating the unknown parameters $\boldsymbol{\xi}$ from the sufficient statistic $\tilde{\mathbf{y}}_{\mathrm{s}}$. According to [36], the FIM $\mathbf{J}\left(\boldsymbol{\xi}\right)$ for estimating $\boldsymbol{\xi}$ can be partitioned as

$$\mathbf{J}\left(\boldsymbol{\xi}\right) = \left[\begin{array}{cc|c} \mathbf{J}_{xx} & \mathbf{J}_{xy} & \mathbf{J}_{x\tilde{\boldsymbol{\beta}}} \\ \mathbf{J}_{xy}^T & \mathbf{J}_{yy} & \mathbf{J}_{y\tilde{\boldsymbol{\beta}}} \\ \hline \mathbf{J}_{x\tilde{\boldsymbol{\beta}}}^T & \mathbf{J}_{y\tilde{\boldsymbol{\beta}}}^T & \mathbf{J}_{\tilde{\boldsymbol{\beta}}\tilde{\boldsymbol{\beta}}} \end{array}\right] \in \mathbb{R}^{4\times 4}, \tag{18}$$

where

$$\mathbf{J}_{xx} = \frac{2T|\beta|^2}{\sigma^2}\mathrm{tr}\left(\dot{\mathbf{A}}_x\mathbf{F}_{\mathrm{A}}\mathbf{F}_{\mathrm{D}}\mathbf{F}_{\mathrm{D}}^H\mathbf{F}_{\mathrm{A}}^H\dot{\mathbf{A}}_x^H\right), \tag{19a}$$

$$\mathbf{J}_{xy} = \frac{2T|\beta|^2}{\sigma^2}\mathrm{tr}\left(\dot{\mathbf{A}}_y\mathbf{F}_{\mathrm{A}}\mathbf{F}_{\mathrm{D}}\mathbf{F}_{\mathrm{D}}^H\mathbf{F}_{\mathrm{A}}^H\dot{\mathbf{A}}_x^H\right), \tag{19b}$$

$$\mathbf{J}_{yy} = \frac{2T|\beta|^2}{\sigma^2}\mathrm{tr}\left(\dot{\mathbf{A}}_y\mathbf{F}_{\mathrm{A}}\mathbf{F}_{\mathrm{D}}\mathbf{F}_{\mathrm{D}}^H\mathbf{F}_{\mathrm{A}}^H\dot{\mathbf{A}}_y^H\right), \tag{19c}$$

$$\mathbf{J}_{x\tilde{\boldsymbol{\beta}}} = \frac{2T}{\sigma^2}\mathrm{Re}\left\{\beta^*\mathrm{tr}(\mathbf{A}\mathbf{F}_{\mathrm{A}}\mathbf{F}_{\mathrm{D}}\mathbf{F}_{\mathrm{D}}^H\mathbf{F}_{\mathrm{A}}^H\dot{\mathbf{A}}_x^H)[1,j]\right\}, \tag{19d}$$

$$\mathbf{J}_{y\tilde{\boldsymbol{\beta}}} = \frac{2T}{\sigma^2}\mathrm{Re}\left\{\beta^*\mathrm{tr}(\mathbf{A}\mathbf{F}_{\mathrm{A}}\mathbf{F}_{\mathrm{D}}\mathbf{F}_{\mathrm{D}}^H\mathbf{F}_{\mathrm{A}}^H\dot{\mathbf{A}}_y^H)[1,j]\right\}, \tag{19e}$$

$$\mathbf{J}_{\tilde{\boldsymbol{\beta}}\tilde{\boldsymbol{\beta}}} = \frac{2T}{\sigma^2}\mathrm{tr}\left(\mathbf{A}\mathbf{F}_{\mathrm{A}}\mathbf{F}_{\mathrm{D}}\mathbf{F}_{\mathrm{D}}^H\mathbf{F}_{\mathrm{A}}^H\mathbf{A}^H\right)\mathbf{I}_2, \tag{19f}$$

and $\dot{\mathbf{A}}_x = \frac{\partial \mathbf{A}}{\partial x}$ and $\dot{\mathbf{A}}_y = \frac{\partial \mathbf{A}}{\partial y}$ denote the partial derivatives of $\mathbf{A}$ with respect to x and y, respectively.

For notational simplicity, we define

$$\mathbf{J}_{11} = \begin{bmatrix} \mathbf{J}_{xx} & \mathbf{J}_{xy} \\ \mathbf{J}_{xy}^T & \mathbf{J}_{yy} \end{bmatrix}, \quad \mathbf{J}_{12} = \begin{bmatrix} \mathbf{J}_{x\tilde{\boldsymbol{\beta}}} \\ \mathbf{J}_{y\tilde{\boldsymbol{\beta}}} \end{bmatrix}, \quad \mathbf{J}_{22} = \mathbf{J}_{\tilde{\boldsymbol{\beta}}\tilde{\boldsymbol{\beta}}}. \tag{20}$$

By isolating the impact of the nuisance parameter $\tilde{\boldsymbol{\beta}}$, the EFIM [28] of the target position $[x,y]^T$ can be expressed as

$$\mathbf{J}_{\mathrm{e}}(x,y) = \mathbf{J}_{11} - \mathbf{J}_{12}\mathbf{J}_{22}^{-1}\mathbf{J}_{12}^T. \tag{21}$$

Therefore, the SPEB of near-field target localization can be represented as

$$\mathrm{SPEB} = \mathrm{tr}\left(\left(\mathbf{J}_{\mathrm{e}}(x,y)\right)^{-1}\right). \tag{22}$$

From (18), (19), (20), (21), and (22), we observe that the SPEB can be expressed as a function of the HBF matrix $\mathbf{F}_{\mathrm{A}}\mathbf{F}_{\mathrm{D}}$. Therefore, we can enhance the target localization accuracy by optimizing the HBF design.

B. Problem Formulation

To investigate the tradeoff between localization accuracy and communication rate, we formulate sensing-oriented optimization and communication-oriented optimization problems as follows.

For the sensing-oriented optimization, we aim to jointly design the digital beamformer and partially-connected analog beamformer to minimize the SPEB of target localization, while ensuring the communication rate requirements of individual CUs, transmit power budget, and constant modulus constraints. The sensing-oriented HBF design can be formulated as

$$\min_{\mathbf{F}_{\mathrm{A}},\mathbf{F}_{\mathrm{D}}} \ \mathrm{SPEB} \tag{23a}$$

$$\text{s.t.} \ \ \mathrm{R}_k \geq \mathrm{R}_{\min,k}, \forall k, \tag{23b}$$

$$\|\mathbf{F}_{\mathrm{A}}\mathbf{F}_{\mathrm{D}}\|_F^2 \leq P, \tag{23c}$$

$$\mathbf{F}_{\mathrm{A}} \in \mathcal{A}, \tag{23d}$$

where $\mathrm{R}_{\min,k}$ denotes the minimum communication rate demand of the k-th CU, P denotes the transmit power budget, and $\mathcal{A}$ denotes the feasible set of partially-connected analog beamformer in which constant modulus constraints are imposed on the nonzero elements of $\mathbf{F}_{\mathrm{A}}$. For convenience, let $\Gamma_k = 2^{\mathrm{R}_{\min,k}} - 1, \forall k$ denote the SINR threshold of the k-th CU.

The communication-oriented HBF design is formulated to maximize the sum-rate of CUs under the target localization accuracy requirement, given by

$$\max_{\mathbf{F}_{\mathrm{A}},\mathbf{F}_{\mathrm{D}}} \sum_{k=1}^{K}\log\left(1+\mathrm{SINR}_k\right) \tag{24a}$$

$$\text{s.t.} \ \ \mathrm{SPEB} \leq \Gamma_s, \tag{24b}$$

$$\|\mathbf{F}_{\mathrm{A}}\mathbf{F}_{\mathrm{D}}\|_F^2 \leq P, \tag{24c}$$

$$\mathbf{F}_{\mathrm{A}} \in \mathcal{A}, \tag{24d}$$

where Γ_s denotes the SPEB threshold of target localization. Note that both (23) and (24) are nonconvex problems, which are difficult to tackle due to the intractable objective function, highly coupled optimization variables, and nonconvex constant modulus constraints.

IV. Sensing-Oriented HBF Design

In this section, we propose an SDR-based BCD algorithm to solve the communication rate-constrained sensing SPEB minimization problem.

A. Problem Reformulation

To tackle the sophisticated objective function in (23a), we introduce an auxiliary positive semidefinite matrix $\mathbf{U} \in \mathbb{C}^{2\times 2}$. By leveraging the Schur complement, (23a) can be equivalently transformed into a tractable problem based on the following proposition.

Proposition 1: Minimizing the SPEB in (23a) is equivalent to solving the following problem in (25), given by

$$\min_{\mathbf{F}_{\mathrm{A}},\mathbf{F}_{\mathrm{D}},\mathbf{U}} \operatorname{tr}\left(\mathbf{U}^{-1}\right) \tag{25a}$$

$$\text{s.t.} \quad \begin{bmatrix} \mathbf{J}_{11}-\mathbf{U} & \mathbf{J}_{12} \\ \mathbf{J}_{12}^{T} & \mathbf{J}_{22} \end{bmatrix} \succeq \mathbf{0}, \tag{25b}$$

$$\mathbf{U} \succeq \mathbf{0}. \tag{25c}$$

With the aid of **Proposition** 1, problem (23) can be equivalently reformulated as

$$\min_{\mathbf{F}_{\mathrm{A}},\mathbf{F}_{\mathrm{D}},\mathbf{U}} \operatorname{tr}\left(\mathbf{U}^{-1}\right) \tag{26a}$$

$$\text{s.t.} \quad \text{(23b), (23c), (23d), (25b), (25c).} \tag{26b}$$

Then, the BCD framework is exploited to decompose problem (26) into the following two subproblems and iteratively solve in an alternating manner.

B. Analog Beamformer Design

In this subsection, we optimize the analog beamformer $\mathbf{F}_{\mathrm{A}}$ with given the digital beamformer $\mathbf{F}_{\mathrm{D}}$. Exploiting the block diagonal structure, the analog beamformer can be recast as

$$\mathbf{F}_{\mathrm{A}} = \tilde{\mathbf{F}}_{\mathrm{A}}\boldsymbol{\Phi} = \operatorname{diag}\left(\mathbf{f}_{\mathrm{A}}\right)\boldsymbol{\Phi}, \tag{27}$$

where $\tilde{\mathbf{F}}_{\mathrm{A}} = \operatorname{blkdiag}\left\{\operatorname{diag}\left(\mathbf{f}_1\right),\ldots,\operatorname{diag}\left(\mathbf{f}_{N_{\mathrm{RF}}}\right)\right\} \in \mathbb{C}^{N\times N}$ and $\mathbf{f}_{\mathrm{A}} = [\mathbf{f}_1^T,\ldots,\mathbf{f}_{N_{\mathrm{RF}}}^T]^T \in \mathbb{C}^{N\times 1}$ represent a diagonal matrix and a column vector consisting of the nonzero elements of $\mathbf{F}_{\mathrm{A}}$, respectively, $\boldsymbol{\Phi} = \operatorname{blkdiag}\left\{\mathbf{1}_M,\ldots,\mathbf{1}_M\right\} \in \mathbb{C}^{N\times N_{\mathrm{RF}}}$ represents a block diagonal matrix in which $\mathbf{1}_M \in \mathbb{C}^{M\times 1}$ represents a column vector with each element being 1. Thus, the transmit covariance matrix in (16) can be rewritten as

$$\begin{aligned}\mathbf{R}_{\mathrm{X}} &= \sum_{k=1}^{K} \operatorname{diag}\left(\mathbf{f}_{\mathrm{A}}\right)\boldsymbol{\Phi}\mathbf{f}_{\mathrm{D},k}\mathbf{f}_{\mathrm{D},k}^{H}\boldsymbol{\Phi}^{H}\operatorname{diag}\left(\mathbf{f}_{\mathrm{A}}\right)^{H} \\ &= \sum_{k=1}^{K} \operatorname{diag}\left(\boldsymbol{\Phi}\mathbf{f}_{\mathrm{D},k}\right)\mathbf{f}_{\mathrm{A}}\mathbf{f}_{\mathrm{A}}^{H}\operatorname{diag}\left(\boldsymbol{\Phi}\mathbf{f}_{\mathrm{D},k}\right)^{H}. \end{aligned} \tag{28}$$

For notational convenience, we define

$$\mathbf{J}_{11}\left(\mathbf{f}_{\mathrm{A}}\right) = \frac{2T|\beta|^2}{\sigma^2}\operatorname{Re}\left\{\begin{bmatrix} \operatorname{tr}(\ddot{\boldsymbol{\Pi}}_{xx}\mathbf{f}_{\mathrm{A}}\mathbf{f}_{\mathrm{A}}^{H}) & \operatorname{tr}(\ddot{\boldsymbol{\Pi}}_{xy}\mathbf{f}_{\mathrm{A}}\mathbf{f}_{\mathrm{A}}^{H}) \\ \operatorname{tr}(\ddot{\boldsymbol{\Pi}}_{xy}^{H}\mathbf{f}_{\mathrm{A}}\mathbf{f}_{\mathrm{A}}^{H}) & \operatorname{tr}(\ddot{\boldsymbol{\Pi}}_{yy}\mathbf{f}_{\mathrm{A}}\mathbf{f}_{\mathrm{A}}^{H}) \end{bmatrix}\right\}, \tag{29a}$$

$$\mathbf{J}_{12}\left(\mathbf{f}_{\mathrm{A}}\right) = \frac{2T}{\sigma^2}\operatorname{Re}\left\{\begin{bmatrix} \beta^{*}\operatorname{tr}(\dot{\boldsymbol{\Pi}}_{x}\mathbf{f}_{\mathrm{A}}\mathbf{f}_{\mathrm{A}}^{H}) \\ \beta^{*}\operatorname{tr}(\dot{\boldsymbol{\Pi}}_{y}\mathbf{f}_{\mathrm{A}}\mathbf{f}_{\mathrm{A}}^{H}) \end{bmatrix}[1,j]\right\}, \tag{29b}$$

$$\mathbf{J}_{22}\left(\mathbf{f}_{\mathrm{A}}\right) = \frac{2T}{\sigma^2}\operatorname{tr}\left(\boldsymbol{\Pi}\mathbf{f}_{\mathrm{A}}\mathbf{f}_{\mathrm{A}}^{H}\right)\mathbf{I}_2, \tag{29c}$$

and

$$\ddot{\boldsymbol{\Pi}}_{xx} = \sum_{k=1}^{K} \operatorname{diag}\left(\boldsymbol{\Phi}\mathbf{f}_{\mathrm{D},k}\right)^{H}\dot{\mathbf{A}}_{x}^{H}\dot{\mathbf{A}}_{x}\operatorname{diag}\left(\boldsymbol{\Phi}\mathbf{f}_{\mathrm{D},k}\right), \tag{30a}$$

$$\ddot{\boldsymbol{\Pi}}_{xy} = \sum_{k=1}^{K} \operatorname{diag}\left(\boldsymbol{\Phi}\mathbf{f}_{\mathrm{D},k}\right)^{H}\dot{\mathbf{A}}_{x}^{H}\dot{\mathbf{A}}_{y}\operatorname{diag}\left(\boldsymbol{\Phi}\mathbf{f}_{\mathrm{D},k}\right), \tag{30b}$$

$$\ddot{\boldsymbol{\Pi}}_{yy} = \sum_{k=1}^{K} \operatorname{diag}\left(\boldsymbol{\Phi}\mathbf{f}_{\mathrm{D},k}\right)^{H}\dot{\mathbf{A}}_{y}^{H}\dot{\mathbf{A}}_{y}\operatorname{diag}\left(\boldsymbol{\Phi}\mathbf{f}_{\mathrm{D},k}\right), \tag{30c}$$

$$\dot{\boldsymbol{\Pi}}_{x} = \sum_{k=1}^{K} \operatorname{diag}\left(\boldsymbol{\Phi}\mathbf{f}_{\mathrm{D},k}\right)^{H}\dot{\mathbf{A}}_{x}^{H}\mathbf{A}\operatorname{diag}\left(\boldsymbol{\Phi}\mathbf{f}_{\mathrm{D},k}\right), \tag{30d}$$

$$\dot{\boldsymbol{\Pi}}_{y} = \sum_{k=1}^{K} \operatorname{diag}\left(\boldsymbol{\Phi}\mathbf{f}_{\mathrm{D},k}\right)^{H}\dot{\mathbf{A}}_{y}^{H}\mathbf{A}\operatorname{diag}\left(\boldsymbol{\Phi}\mathbf{f}_{\mathrm{D},k}\right), \tag{30e}$$

$$\boldsymbol{\Pi} = \sum_{k=1}^{K} \operatorname{diag}\left(\boldsymbol{\Phi}\mathbf{f}_{\mathrm{D},k}\right)^{H}\mathbf{A}^{H}\mathbf{A}\operatorname{diag}\left(\boldsymbol{\Phi}\mathbf{f}_{\mathrm{D},k}\right), \tag{30f}$$

$$\bar{\mathbf{H}}_{k,j} = \operatorname{diag}\left(\boldsymbol{\Phi}\mathbf{f}_{\mathrm{D},j}\right)^{H}\mathbf{h}_k\mathbf{h}_k^{H}\operatorname{diag}\left(\boldsymbol{\Phi}\mathbf{f}_{\mathrm{D},j}\right). \tag{30g}$$

Therefore, the subproblem with respect to $\mathbf{f}_{\mathrm{A}}$ can be formulated as

$$\min_{\mathbf{f}_{\mathrm{A}},\mathbf{U}} \operatorname{tr}\left(\mathbf{U}^{-1}\right) \tag{31a}$$

$$\text{s.t.} \quad \begin{bmatrix} \mathbf{J}_{11}\left(\mathbf{f}_{\mathrm{A}}\right)-\mathbf{U} & \mathbf{J}_{12}\left(\mathbf{f}_{\mathrm{A}}\right) \\ \mathbf{J}_{12}^{T}\left(\mathbf{f}_{\mathrm{A}}\right) & \mathbf{J}_{22}\left(\mathbf{f}_{\mathrm{A}}\right) \end{bmatrix} \succeq \mathbf{0}, \tag{31b}$$

$$(1+\frac{1}{\Gamma_k})\mathbf{f}_{\mathrm{A}}^{H}\bar{\mathbf{H}}_{k,k}\mathbf{f}_{\mathrm{A}} \geq \sum_{j=1}^{K}\mathbf{f}_{\mathrm{A}}^{H}\bar{\mathbf{H}}_{k,j}\mathbf{f}_{\mathrm{A}}+\sigma^2, \forall k, \tag{31c}$$

$$\left|\left[\mathbf{f}_{\mathrm{A}}\right]_i\right| = 1, \forall i, \tag{31d}$$

$$\text{(25c).} \tag{31e}$$

It is observed that problem (31) is nonconvex due to the quadratic constraints in (31b) and (31c), and the constant modulus constraints in (31d). Therefore, the SDR technique [37] is exploited to tackle the nonconvexity of problem (31). Specifically, we define the auxiliary variable $\mathbf{R}_{\mathrm{A}} = \mathbf{f}_{\mathrm{A}}\mathbf{f}_{\mathrm{A}}^{H}$ such that $\mathbf{R}_{\mathrm{A}} \succeq \mathbf{0}$ and $\operatorname{rank}\left(\mathbf{R}_{\mathrm{A}}\right) = 1$. By dropping the nonconvex rank-one constraint, problem (31) can be relaxed as

$$\min_{\mathbf{R}_{\mathrm{A}},\mathbf{U}} \operatorname{tr}\left(\mathbf{U}^{-1}\right) \tag{32a}$$

$$\text{s.t.} \quad \begin{bmatrix} \mathbf{J}_{11}\left(\mathbf{R}_{\mathrm{A}}\right)-\mathbf{U} & \mathbf{J}_{12}\left(\mathbf{R}_{\mathrm{A}}\right) \\ \mathbf{J}_{12}^{T}\left(\mathbf{R}_{\mathrm{A}}\right) & \mathbf{J}_{22}\left(\mathbf{R}_{\mathrm{A}}\right) \end{bmatrix} \succeq \mathbf{0}, \tag{32b}$$

$$(1+\frac{1}{\Gamma_k})\operatorname{tr}\left(\bar{\mathbf{H}}_{k,k}\mathbf{R}_{\mathrm{A}}\right) \geq \sum_{j=1}^{K}\operatorname{tr}\left(\bar{\mathbf{H}}_{k,j}\mathbf{R}_{\mathrm{A}}\right)+\sigma^2, \forall k, \tag{32c}$$

$$\left|\left[\mathbf{R}_{\mathrm{A}}\right]_{i,i}\right| = 1, \forall i, \tag{32d}$$

$$\mathbf{R}_{\mathrm{A}} \succeq \mathbf{0}, \tag{32e}$$

$$\text{(25c),} \tag{32f}$$

where we define

$$\mathbf{J}_{11}\left(\mathbf{R}_{\mathrm{A}}\right) = \frac{2T|\beta|^2}{\sigma^2}\operatorname{Re}\left\{\begin{bmatrix} \operatorname{tr}(\ddot{\boldsymbol{\Pi}}_{xx}\mathbf{R}_{\mathrm{A}}) & \operatorname{tr}(\ddot{\boldsymbol{\Pi}}_{xy}\mathbf{R}_{\mathrm{A}}) \\ \operatorname{tr}(\ddot{\boldsymbol{\Pi}}_{xy}^{H}\mathbf{R}_{\mathrm{A}}) & \operatorname{tr}(\ddot{\boldsymbol{\Pi}}_{yy}\mathbf{R}_{\mathrm{A}}) \end{bmatrix}\right\}, \tag{33a}$$

$$\mathbf{J}_{12}\left(\mathbf{R}_{\mathrm{A}}\right) = \frac{2T}{\sigma^2}\operatorname{Re}\left\{\begin{bmatrix} \beta^{*}\operatorname{tr}(\dot{\boldsymbol{\Pi}}_{x}\mathbf{R}_{\mathrm{A}}) \\ \beta^{*}\operatorname{tr}(\dot{\boldsymbol{\Pi}}_{y}\mathbf{R}_{\mathrm{A}}) \end{bmatrix}[1,j]\right\}, \tag{33b}$$

$$\mathbf{J}_{22}\left(\mathbf{R}_{\mathrm{A}}\right) = \frac{2T}{\sigma^2}\operatorname{tr}\left(\boldsymbol{\Pi}\mathbf{R}_{\mathrm{A}}\right)\mathbf{I}_2, \tag{33c}$$

We observe that problem (32) is a convex semidefinite programming (SDP) problem, whose optimal solution can be efficiently acquired by CVX. Let $\mathbf{R}_{\mathrm{A}}^{\star}$ denote the optimal solution to problem (32). However, the rank of $\mathbf{R}_{\mathrm{A}}^{\star}$ may be larger than one due to the omission of the rank-one constraint in problem (32). Therefore, we reconstruct a feasible rank-one solution by leveraging Gaussian randomization [37].

C. Digital Beamformer Design

In this subsection, we optimize the digital beamformer $\mathbf{F}_{\mathrm{D}}$ with given the analog beamformer $\mathbf{F}_{\mathrm{A}}$. Taking into account the block diagonal structure of $\mathbf{F}_{\mathrm{A}}$, the transmit power can be rewritten as

$$\|\mathbf{F}_{\mathrm{A}}\mathbf{F}_{\mathrm{D}}\|_F^2 = \mathrm{tr}\left(\mathbf{F}_{\mathrm{A}}^H\mathbf{F}_{\mathrm{A}}\mathbf{F}_{\mathrm{D}}\mathbf{F}_{\mathrm{D}}^H\right) = M\mathrm{tr}\left(\mathbf{F}_{\mathrm{D}}\mathbf{F}_{\mathrm{D}}^H\right). \quad (34)$$

The subproblem with respect to $\mathbf{F}_{\mathrm{D}}$ can be reformulated as

$$\min_{\mathbf{F}_{\mathrm{D}},\mathbf{U}} \mathrm{tr}\left(\mathbf{U}^{-1}\right) \quad (35a)$$

$$\text{s.t.} \begin{bmatrix} \mathbf{J}_{11}\left(\mathbf{F}_{\mathrm{D}}\right)-\mathbf{U} & \mathbf{J}_{12}\left(\mathbf{F}_{\mathrm{D}}\right) \\ \mathbf{J}_{12}^T\left(\mathbf{F}_{\mathrm{D}}\right) & \mathbf{J}_{22}\left(\mathbf{F}_{\mathrm{D}}\right) \end{bmatrix} \succeq \mathbf{0}, \quad (35b)$$

$$(1+\frac{1}{\Gamma_k})\mathbf{f}_{\mathrm{D},k}^H\tilde{\mathbf{H}}_k\mathbf{f}_{\mathrm{D},k} \geq \sum_{j=1}^{K}\mathbf{f}_{\mathrm{D},j}^H\tilde{\mathbf{H}}_k\mathbf{f}_{\mathrm{D},j}+\sigma^2, \forall k, \quad (35c)$$

$$\mathrm{tr}\left(\mathbf{F}_{\mathrm{D}}\mathbf{F}_{\mathrm{D}}^H\right) \leq P/M, \quad (35d)$$

(25c), (35e)

where we define

$$\mathbf{J}_{11}\left(\mathbf{F}_{\mathrm{D}}\right)=\frac{2T|\beta|^2}{\sigma^2}\mathrm{Re}\left\{\begin{bmatrix}\mathrm{tr}(\ddot{\mathbf{\Psi}}_{xx}\mathbf{F}_{\mathrm{D}}\mathbf{F}_{\mathrm{D}}^H) & \mathrm{tr}(\ddot{\mathbf{\Psi}}_{xy}\mathbf{F}_{\mathrm{D}}\mathbf{F}_{\mathrm{D}}^H)\\ \mathrm{tr}(\ddot{\mathbf{\Psi}}_{xy}^H\mathbf{F}_{\mathrm{D}}\mathbf{F}_{\mathrm{D}}^H) & \mathrm{tr}(\ddot{\mathbf{\Psi}}_{yy}\mathbf{F}_{\mathrm{D}}\mathbf{F}_{\mathrm{D}}^H)\end{bmatrix}\right\}, \quad (36a)$$

$$\mathbf{J}_{12}\left(\mathbf{F}_{\mathrm{D}}\right)=\frac{2T}{\sigma^2}\mathrm{Re}\left\{\begin{bmatrix}\beta^*\mathrm{tr}(\dot{\mathbf{\Psi}}_x\mathbf{F}_{\mathrm{D}}\mathbf{F}_{\mathrm{D}}^H)\\ \beta^*\mathrm{tr}(\dot{\mathbf{\Psi}}_y\mathbf{F}_{\mathrm{D}}\mathbf{F}_{\mathrm{D}}^H)\end{bmatrix}[1,j]\right\}, \quad (36b)$$

$$\mathbf{J}_{22}\left(\mathbf{F}_{\mathrm{D}}\right)=\frac{2T}{\sigma^2}\mathrm{tr}\left(\mathbf{\Psi}\mathbf{F}_{\mathrm{D}}\mathbf{F}_{\mathrm{D}}^H\right)\mathbf{I}_2, \quad (36c)$$

and

$$\ddot{\mathbf{\Psi}}_{xx}=\mathbf{F}_{\mathrm{A}}^H\dot{\mathbf{A}}_x^H\dot{\mathbf{A}}_x\mathbf{F}_{\mathrm{A}}, \quad (37a)$$

$$\ddot{\mathbf{\Psi}}_{xy}=\mathbf{F}_{\mathrm{A}}^H\dot{\mathbf{A}}_x^H\dot{\mathbf{A}}_y\mathbf{F}_{\mathrm{A}}, \quad (37b)$$

$$\ddot{\mathbf{\Psi}}_{yy}=\mathbf{F}_{\mathrm{A}}^H\dot{\mathbf{A}}_y^H\dot{\mathbf{A}}_y\mathbf{F}_{\mathrm{A}}, \quad (37c)$$

$$\dot{\mathbf{\Psi}}_{x}=\mathbf{F}_{\mathrm{A}}^H\dot{\mathbf{A}}_x^H\mathbf{A}\mathbf{F}_{\mathrm{A}}, \quad (37d)$$

$$\dot{\mathbf{\Psi}}_{y}=\mathbf{F}_{\mathrm{A}}^H\dot{\mathbf{A}}_y^H\mathbf{A}\mathbf{F}_{\mathrm{A}}, \quad (37e)$$

$$\mathbf{\Psi}=\mathbf{F}_{\mathrm{A}}^H\mathbf{A}^H\mathbf{A}\mathbf{F}_{\mathrm{A}}, \quad (37f)$$

$$\tilde{\mathbf{H}}_k=\mathbf{F}_{\mathrm{A}}^H\mathbf{h}_k\mathbf{h}_k^H\mathbf{F}_{\mathrm{A}}. \quad (37g)$$

Note that problem (35) is nonconvex since the quadratic constraints in (35b) and (35c) are nonconvex with respect to $\mathbf{F}_{\mathrm{D}}$. Thus, we adopt the SDR technique [37] to handle the nonconvex problem in (35). In particular, we define the auxiliary variables $\mathbf{R}_{\mathrm{D},k}=\mathbf{f}_{\mathrm{D},k}\mathbf{f}_{\mathrm{D},k}^H, \forall k$ such that $\mathbf{R}_{\mathrm{D},k}\succeq\mathbf{0}$ and $\mathrm{rank}\left(\mathbf{R}_{\mathrm{D},k}\right)=1, \forall k$. By omitting the nonconvex rank-one constraints, the SDR problem of problem (35) can be represented as

$$\min_{\mathbf{R}_{\mathrm{D},k},\mathbf{U}} \mathrm{tr}\left(\mathbf{U}^{-1}\right) \quad (38a)$$

$$\text{s.t.} \begin{bmatrix} \mathbf{J}_{11}\left(\mathbf{R}_{\mathrm{D},k}\right)-\mathbf{U} & \mathbf{J}_{12}\left(\mathbf{R}_{\mathrm{D},k}\right) \\ \mathbf{J}_{12}^T\left(\mathbf{R}_{\mathrm{D},k}\right) & \mathbf{J}_{22}\left(\mathbf{R}_{\mathrm{D},k}\right) \end{bmatrix} \succeq \mathbf{0}, \quad (38b)$$

$$(1+\frac{1}{\Gamma_k})\mathrm{tr}\left(\tilde{\mathbf{H}}_k\mathbf{R}_{\mathrm{D},k}\right) \geq \sum_{j=1}^{K}\mathrm{tr}\left(\tilde{\mathbf{H}}_k\mathbf{R}_{\mathrm{D},j}\right)+\sigma^2, \forall k, \quad (38c)$$

$$\mathrm{tr}\left(\sum_{k=1}^{K}\mathbf{R}_{\mathrm{D},k}\right) \leq P/M, \quad (38d)$$

$$\mathbf{R}_{\mathrm{D},k}\succeq\mathbf{0}, \forall k, \quad (38e)$$

(25c), (38f)

where we define

$$\mathbf{J}_{11}(\mathbf{R}_{\mathrm{D},k})=\frac{2T|\beta|^2}{\sigma^2}\mathrm{Re}\left\{\begin{bmatrix}\mathrm{tr}(\ddot{\mathbf{\Psi}}_{xx}\sum_{k=1}^{K}\mathbf{R}_{\mathrm{D},k}) & \mathrm{tr}(\ddot{\mathbf{\Psi}}_{xy}\sum_{k=1}^{K}\mathbf{R}_{\mathrm{D},k})\\ \mathrm{tr}(\ddot{\mathbf{\Psi}}_{xy}^H\sum_{k=1}^{K}\mathbf{R}_{\mathrm{D},k}) & \mathrm{tr}(\ddot{\mathbf{\Psi}}_{yy}\sum_{k=1}^{K}\mathbf{R}_{\mathrm{D},k})\end{bmatrix}\right\}, \quad (39a)$$

$$\mathbf{J}_{12}\left(\mathbf{R}_{\mathrm{D},k}\right)=\frac{2T}{\sigma^2}\mathrm{Re}\left\{\begin{bmatrix}\beta^*\mathrm{tr}(\dot{\mathbf{\Psi}}_x\sum_{k=1}^{K}\mathbf{R}_{\mathrm{D},k})\\ \beta^*\mathrm{tr}(\dot{\mathbf{\Psi}}_y\sum_{k=1}^{K}\mathbf{R}_{\mathrm{D},k})\end{bmatrix}[1,j]\right\}, \quad (39b)$$

$$\mathbf{J}_{22}\left(\mathbf{R}_{\mathrm{D},k}\right)=\frac{2T}{\sigma^2}\mathrm{tr}\left(\mathbf{\Psi}\sum_{k=1}^{K}\mathbf{R}_{\mathrm{D},k}\right)\mathbf{I}_2. \quad (39c)$$

Problem (38) is a convex SDP problem, which can be efficiently solved by CVX. Let $\mathbf{R}_{\mathrm{D},k}^\star, \forall k$ denote the optimal solution to problem (38). Nevertheless, $\mathbf{R}_{\mathrm{D},k}^\star, \forall k$ may not satisfy the rank-one constraints. Therefore, eigenvalue decomposition [37] is applied to extract a feasible rank-one solution to problem (35) from $\mathbf{R}_{\mathrm{D},k}^\star$.

Algorithm 1 Proposed SDR-BCD Algorithm for Solving Problem (23)

1: **Input:** Digital beamformer $\mathbf{F}_{\mathrm{D}}^{(0)}$, iteration index $n=1$, and convergence tolerance δ.
2: **repeat**
3: Update $\mathbf{F}_{\mathrm{A}}^{(n)}$ by solving problem (32);
4: Update $\mathbf{F}_{\mathrm{D}}^{(n)}$ by solving problem (38);
5: $n=n+1$;
6: **until** The objective value of problem (23) is converged.
7: **Output:** $\mathbf{F}_{\mathrm{A}}$, $\mathbf{F}_{\mathrm{D}}$.

D. Overall Algorithm

Following the aforementioned design, the analog beamformer and digital beamformer are alternately updated until convergence. The proposed SDR-BCD algorithm for solving communication rate-constrained SPEB minimization problem (23) is summarized in **Algorithm 1**. The digital beamformer is initialized with an arbitrary $N_{\mathrm{RF}}\times K$ dimensional matrix that satisfies power constraints.

1) Convergence Analysis: The optimal solutions of SDP problems (32) and (38) are obtained by utilizing CVX. Nevertheless, constructing the rank-one solution by adopting Gaussian randomization or eigenvalue decomposition inevitably causes slight performance loss, thus failing to theoretically guarantee the monotonicity of objective value [38]. In practice, the proposed SDR-BCD algorithm generally converges to a stationary point of problem (23).

2) Complexity Analysis: The computational complexity of **Algorithm** 1 is dominant by that of solving SDP problems (32) and (38) via the interior point method [39]. Given a solution accuracy ϵ, the computational complexities for solving problem (32) and problem (38) are given by $\mathcal{O}\left(\log\left(1/\epsilon\right)N^{4.5}\right)$ and $\mathcal{O}\left(\log\left(1/\epsilon\right)K^{4.5}N_{\mathrm{RF}}^{4.5}\right)$, respectively. Thus, the total computational complexity of **Algorithm** 1 is given by $\mathcal{O}\left(N_{\mathrm{iter}}\log\left(1/\epsilon\right)\left(N^{4.5}+K^{4.5}N_{\mathrm{RF}}^{4.5}\right)\right)$, where N_{iter} denotes the number of iterations.

V. Communication-Oriented HBF Design

This section proposes an SCA-based BCD algorithm to address the sensing SPEB-constrained communication sum-rate maximization problem.

A. Problem Reformulation

The objective function of problem (24) is intractable due to its sum-of-logarithm-of-ratio form. We reformulate problem (24) as a tractable one by exploiting the FP technique. First, the objective function in (24a) is transformed into a sum-of-ratio form by adopting the Lagrangian dual transform [40]. By introducing the auxiliary variable $\boldsymbol{\gamma}=\left[\gamma_1,\ldots,\gamma_K\right]^T\in\mathbb{R}_+^{K\times 1}$, the objective function in (24a) can be equivalently recast as

$$\sum_{k=1}^{K}\log\left(1+\gamma_k\right)-\sum_{k=1}^{K}\gamma_k+\sum_{k=1}^{K}\frac{\left(1+\gamma_k\right)\left|\mathbf{h}_k^H\mathbf{F}_{\mathrm{A}}\mathbf{f}_{\mathrm{D},k}\right|^2}{\sum_{j=1}^{K}\left|\mathbf{h}_k^H\mathbf{F}_{\mathrm{A}}\mathbf{f}_{\mathrm{D},j}\right|^2+\sigma^2}. \tag{40}$$

Then, the quadratic transform [40] is employed to handle the sum-of-ratio term in (40). By introducing the auxiliary variable $\boldsymbol{\mu}=\left[\mu_1,\ldots,\mu_K\right]^T\in\mathbb{C}^{K\times 1}$, problem (24) can be reformulated as

$$\max_{\mathbf{F}_{\mathrm{A}},\mathbf{F}_{\mathrm{D}},\boldsymbol{\gamma},\boldsymbol{\mu}} f\left(\mathbf{F}_{\mathrm{A}},\mathbf{F}_{\mathrm{D}},\boldsymbol{\gamma},\boldsymbol{\mu}\right) \tag{41a}$$

$$\text{s.t.}\quad (24b),(24c),(24d), \tag{41b}$$

where the objective function $f\left(\mathbf{F}_{\mathrm{A}},\mathbf{F}_{\mathrm{D}},\boldsymbol{\gamma},\boldsymbol{\mu}\right)$ in (41a) can be represented as

$$\begin{aligned}f\left(\mathbf{F}_{\mathrm{A}},\mathbf{F}_{\mathrm{D}},\boldsymbol{\gamma},\boldsymbol{\mu}\right)=&\sum_{k=1}^{K}\log\left(1+\gamma_k\right)-\sum_{k=1}^{K}\gamma_k\\&+\sum_{k=1}^{K}2\sqrt{\left(1+\gamma_k\right)}\mathrm{Re}\left\{\mu_k^*\mathbf{h}_k^H\mathbf{F}_{\mathrm{A}}\mathbf{f}_{\mathrm{D},k}\right\}\\&-\sum_{k=1}^{K}\left|\mu_k\right|^2\left(\sum_{j=1}^{K}\left|\mathbf{h}_k^H\mathbf{F}_{\mathrm{A}}\mathbf{f}_{\mathrm{D},j}\right|^2+\sigma^2\right).\end{aligned} \tag{42}$$

To solve problem (41), the BCD framework is applied to optimize the analog beamformer $\mathbf{F}_{\mathrm{A}}$, digital beamformer $\mathbf{F}_{\mathrm{D}}$, and auxiliary variables $\boldsymbol{\gamma}$ and $\boldsymbol{\mu}$ in an alternating fashion. The specific steps for updating the above variables are presented as follows.

With the other variables fixed, the subproblem with respect to γ_k is an unconstrained convex problem. Based on the first-order optimality condition, the optimal solution of γ_k can be given by

$$\gamma_k=\frac{\left|\mathbf{h}_k^H\mathbf{F}_{\mathrm{A}}\mathbf{f}_{\mathrm{D},k}\right|^2}{\sum_{j=1,j\neq k}^{K}\left|\mathbf{h}_k^H\mathbf{F}_{\mathrm{A}}\mathbf{f}_{\mathrm{D},j}\right|^2+\sigma^2},\forall k. \tag{43}$$

Similarly, the optimal solution of μ_k can be computed by solving $\partial f\left(\mathbf{F}_{\mathrm{A}},\mathbf{F}_{\mathrm{D}},\boldsymbol{\gamma},\boldsymbol{\mu}\right)/\partial\mu_k=0$ as

$$\mu_k=\frac{\sqrt{\left(1+\gamma_k\right)}\mathbf{h}_k^H\mathbf{F}_{\mathrm{A}}\mathbf{f}_{\mathrm{D},k}}{\sum_{j=1}^{K}\left|\mathbf{h}_k^H\mathbf{F}_{\mathrm{A}}\mathbf{f}_{\mathrm{D},j}\right|^2+\sigma^2},\forall k. \tag{44}$$

B. Analog Beamformer Design

We design the analog beamformer $\mathbf{F}_{\mathrm{A}}$ with the digital beamformer $\mathbf{F}_{\mathrm{D}}$ and the auxiliary variables $\boldsymbol{\gamma}$ and $\boldsymbol{\mu}$ fixed. To tackle the complicated constraint in (24b), we introduce the auxiliary positive semidefinite matrix $\mathbf{U}\in\mathbb{C}^{2\times 2}$ as shown in Section IV-A. With the block diagonal structure, the subproblem with respect to $\mathbf{F}_{\mathrm{A}}$ can be equivalently reformulated as the subproblem with respect to $\mathbf{f}_{\mathrm{A}}$, given by

$$\min_{\mathbf{f}_{\mathrm{A}},\mathbf{U}}\ \mathbf{f}_{\mathrm{A}}^H\mathbf{B}\mathbf{f}_{\mathrm{A}}-2\mathrm{Re}\left\{\mathbf{f}_{\mathrm{A}}^H\mathbf{c}\right\} \tag{45a}$$

$$\text{s.t. }\mathrm{tr}\left(\mathbf{U}^{-1}\right)\leq\Gamma_s, \tag{45b}$$

$$\mathbf{U}\succeq\mathbf{0}, \tag{45c}$$

$$\begin{bmatrix}\mathbf{J}_{11}\left(\mathbf{f}_{\mathrm{A}}\right)-\mathbf{U} & \mathbf{J}_{12}\left(\mathbf{f}_{\mathrm{A}}\right)\\ \mathbf{J}_{12}^T\left(\mathbf{f}_{\mathrm{A}}\right) & \mathbf{J}_{22}\left(\mathbf{f}_{\mathrm{A}}\right)\end{bmatrix}\succeq\mathbf{0}, \tag{45d}$$

$$\left|\left[\mathbf{f}_{\mathrm{A}}\right]_i\right|=1,\forall i, \tag{45e}$$

where we define

$$\mathbf{B}=\sum_{j=1}^{K}\mathrm{diag}\left(\boldsymbol{\Phi}\mathbf{f}_{\mathrm{D},j}\right)^H\left(\sum_{k=1}^{K}\left|\mu_k\right|^2\mathbf{h}_k\mathbf{h}_k^H\right)\mathrm{diag}\left(\boldsymbol{\Phi}\mathbf{f}_{\mathrm{D},j}\right), \tag{46a}$$

$$\mathbf{c}=\sum_{k=1}^{K}\sqrt{\left(1+\gamma_k\right)}\mu_k\mathrm{diag}\left(\boldsymbol{\Phi}\mathbf{f}_{\mathrm{D},j}\right)^H\mathbf{h}_k. \tag{46b}$$

Note that problem (45) is a nonconvex quadratically constrained quadratic programming (QCQP) problem due to the quadratic objective function in (45a), nonconvex quadratic constraint in (45d), and nonconvex constant modulus constraints in (45e). To address the nonconvex problem, we introduce the auxiliary variable $\mathbf{R}_{\mathrm{A}}=\mathbf{f}_{\mathrm{A}}\mathbf{f}_{\mathrm{A}}^H$ that satisfies $\mathbf{R}_{\mathrm{A}}\succeq\mathbf{0}$ and $\mathrm{rank}\left(\mathbf{R}_{\mathrm{A}}\right)=1$. By omitting $\mathrm{rank}\left(\mathbf{R}_{\mathrm{A}}\right)=1$, problem (45) can be relaxed as

$$\min_{\mathbf{R}_{\mathrm{A}},\mathbf{f}_{\mathrm{A}},\mathbf{U}}\ \mathrm{tr}\left(\mathbf{B}\mathbf{R}_{\mathrm{A}}\right)-2\mathrm{Re}\left\{\mathbf{f}_{\mathrm{A}}^H\mathbf{c}\right\} \tag{47a}$$

$$\text{s.t. }\begin{bmatrix}\mathbf{J}_{11}\left(\mathbf{R}_{\mathrm{A}}\right)-\mathbf{U} & \mathbf{J}_{12}\left(\mathbf{R}_{\mathrm{A}}\right)\\ \mathbf{J}_{12}^T\left(\mathbf{R}_{\mathrm{A}}\right) & \mathbf{J}_{22}\left(\mathbf{R}_{\mathrm{A}}\right)\end{bmatrix}\succeq\mathbf{0}, \tag{47b}$$

$$\left|\left[\mathbf{R}_{\mathrm{A}}\right]_{i,i}\right|=1,\forall i, \tag{47c}$$

$$\mathbf{R}_{\mathrm{A}}\succeq\mathbf{0}, \tag{47d}$$

$$\mathbf{R}_{\mathrm{A}}=\mathbf{f}_{\mathrm{A}}\mathbf{f}_{\mathrm{A}}^H, \tag{47e}$$

$$(45b),(45c). \tag{47f}$$

Nevertheless, problem (47) is still intractable owing to the nonconvex equality constraint in (47e). According to [41],

the equality constraint $\mathbf{R}_{\mathrm{A}} = \mathbf{f}_{\mathrm{A}}\mathbf{f}_{\mathrm{A}}^H$ can be equivalently transformed into the two inequality constraints as follows:

$$\begin{bmatrix} \mathbf{R}_{\mathrm{A}} & \mathbf{f}_{\mathrm{A}} \\ \mathbf{f}_{\mathrm{A}}^H & 1 \end{bmatrix} \succeq \mathbf{0}, \tag{48a}$$

$$\mathrm{tr}\left(\mathbf{R}_{\mathrm{A}}\right) - \mathbf{f}_{\mathrm{A}}^H\mathbf{f}_{\mathrm{A}} \leq 0. \tag{48b}$$

However, constraint (48b) is still nonconvex. We observe that the left-hand-side of constraint (48b) is a difference of convex function. Therefore, we adopt the convex-concave procedure (CCP) method to reserve the convex part $\mathrm{tr}\left(\mathbf{R}_{\mathrm{A}}\right)$ and tackle the concave part $-\mathbf{f}_{\mathrm{A}}^H\mathbf{f}_{\mathrm{A}}$. The SCA technique is applied to obtain the convex approximation of constraint (48b). By taking the first-order Taylor expansion, the upper bound of $-\mathbf{f}_{\mathrm{A}}^H\mathbf{f}_{\mathrm{A}}$ can be approximated as

$$-\mathbf{f}_{\mathrm{A}}^H\mathbf{f}_{\mathrm{A}} \leq -2\mathrm{Re}\left\{\left(\mathbf{f}_{\mathrm{A}}^{(t)}\right)^H\mathbf{f}_{\mathrm{A}}\right\} + \left(\mathbf{f}_{\mathrm{A}}^{(t)}\right)^H\mathbf{f}_{\mathrm{A}}^{(t)}, \tag{49}$$

where $\mathbf{f}_{\mathrm{A}}^{(t)}$ is the solution obtained at the t-th iteration. Thus, the convex approximation of constraint (48b) can be represented as

$$\mathrm{tr}\left(\mathbf{R}_{\mathrm{A}}\right) - 2\mathrm{Re}\left\{\left(\mathbf{f}_{\mathrm{A}}^{(t)}\right)^H\mathbf{f}_{\mathrm{A}}\right\} + \left(\mathbf{f}_{\mathrm{A}}^{(t)}\right)^H\mathbf{f}_{\mathrm{A}}^{(t)} \leq 0. \tag{50}$$

Therefore, the convex approximation of problem (47) can be reformulated as

$$\min_{\mathbf{R}_{\mathrm{A}},\mathbf{f}_{\mathrm{A}},\mathbf{U}} \mathrm{tr}\left(\mathbf{B}\mathbf{R}_{\mathrm{A}}\right) - 2\mathrm{Re}\left\{\mathbf{f}_{\mathrm{A}}^H\mathbf{c}\right\} \tag{51a}$$

$$\text{s.t.} \quad (45b), (45c), (47b), (47c), (47d), (48a), (50). \tag{51b}$$

We observe that problem (51) is a convex problem, which can be efficiently solved by CVX.

C. Digital Beamformer Design

With the analog beamformer $\mathbf{F}_{\mathrm{A}}$ and the auxiliary variables $\boldsymbol{\gamma}$ and $\boldsymbol{\mu}$ fixed, we optimize the digital beamformer $\mathbf{F}_{\mathrm{D}}$. The subproblem with respect to $\mathbf{F}_{\mathrm{D}}$ can be equivalently reformulated as

$$\min_{\mathbf{F}_{\mathrm{D}},\mathbf{U}} \sum_{k=1}^{K}\mathbf{f}_{\mathrm{D},k}^H\mathbf{D}\mathbf{f}_{\mathrm{D},k} - \sum_{k=1}^{K}2\mathrm{Re}\left\{\mathbf{f}_{\mathrm{D},k}^H\mathbf{e}_k\right\} \tag{52a}$$

$$\text{s.t. } \mathrm{tr}\left(\mathbf{U}^{-1}\right) \leq \Gamma_s, \tag{52b}$$

$$\mathbf{U} \succeq \mathbf{0}, \tag{52c}$$

$$\begin{bmatrix} \mathbf{J}_{11}\left(\mathbf{F}_{\mathrm{D}}\right) - \mathbf{U} & \mathbf{J}_{12}\left(\mathbf{F}_{\mathrm{D}}\right) \\ \mathbf{J}_{12}^T\left(\mathbf{F}_{\mathrm{D}}\right) & \mathbf{J}_{22}\left(\mathbf{F}_{\mathrm{D}}\right) \end{bmatrix} \succeq \mathbf{0}, \tag{52d}$$

$$\mathrm{tr}\left(\mathbf{F}_{\mathrm{D}}\mathbf{F}_{\mathrm{D}}^H\right) \leq P/M, \tag{52e}$$

where we define

$$\mathbf{D} = \sum_{k=1}^{K}\left|\mu_k\right|^2\mathbf{F}_{\mathrm{A}}^H\mathbf{h}_k\mathbf{h}_k^H\mathbf{F}_{\mathrm{A}}, \tag{53a}$$

$$\mathbf{e}_k = \sqrt{(1+\gamma_k)}\mu_k\mathbf{F}_{\mathrm{A}}^H\mathbf{h}_k. \tag{53b}$$

Problem (52) is also a nonconvex QCQP problem due to the quadratic objective function in (52a) and the nonconvex quadratic constraint in (52d). To tackle this problem, we introduce the auxiliary variables $\mathbf{R}_{\mathrm{D},k} = \mathbf{f}_{\mathrm{D},k}\mathbf{f}_{\mathrm{D},k}^H, \forall k$ such that $\mathbf{R}_{\mathrm{D},k} \succeq \mathbf{0}$ and $\mathrm{rank}\left(\mathbf{R}_{\mathrm{D},k}\right) = 1, \forall k$. Then, we drop $\mathrm{rank}\left(\mathbf{R}_{\mathrm{D},k}\right) = 1, \forall k$ and obtain the relaxed version of problem (52) as

$$\min_{\mathbf{R}_{\mathrm{D},k},\mathbf{f}_{\mathrm{D},k},\mathbf{U}} \mathrm{tr}\left(\mathbf{D}\sum_{k=1}^{K}\mathbf{R}_{\mathrm{D},k}\right) - \sum_{k=1}^{K}2\mathrm{Re}\left\{\mathbf{f}_{\mathrm{D},k}^H\mathbf{e}_k\right\} \tag{54a}$$

$$\text{s.t.} \quad \begin{bmatrix} \mathbf{J}_{11}\left(\mathbf{R}_{\mathrm{D},k}\right) - \mathbf{U} & \mathbf{J}_{12}\left(\mathbf{R}_{\mathrm{D},k}\right) \\ \mathbf{J}_{12}^T\left(\mathbf{R}_{\mathrm{D},k}\right) & \mathbf{J}_{22}\left(\mathbf{R}_{\mathrm{D},k}\right) \end{bmatrix} \succeq \mathbf{0}, \tag{54b}$$

$$\mathrm{tr}\left(\sum_{k=1}^{K}\mathbf{R}_{\mathrm{D},k}\right) \leq P/M, \tag{54c}$$

$$\mathbf{R}_{\mathrm{D},k} = \mathbf{f}_{\mathrm{D},k}\mathbf{f}_{\mathrm{D},k}^H, \forall k, \tag{54d}$$

$$\mathbf{R}_{\mathrm{D},k} \succeq \mathbf{0}, \forall k, \tag{54e}$$

$$(52b), (52c). \tag{54f}$$

Notice that problem (54) is still nonconvex since the equality constraint in (54d) is nonconvex. The equality constraint $\mathbf{R}_{\mathrm{D},k} = \mathbf{f}_{\mathrm{D},k}\mathbf{f}_{\mathrm{D},k}^H, \forall k$ can be equivalently converted into the following two inequality constraints, given by

$$\begin{bmatrix} \mathbf{R}_{\mathrm{D},k} & \mathbf{f}_{\mathrm{D},k} \\ \mathbf{f}_{\mathrm{D},k}^H & 1 \end{bmatrix} \succeq \mathbf{0}, \forall k, \tag{55a}$$

$$\mathrm{tr}\left(\mathbf{R}_{\mathrm{D},k}\right) - \mathbf{f}_{\mathrm{D},k}^H\mathbf{f}_{\mathrm{D},k} \leq 0, \forall k. \tag{55b}$$

By utilizing the CCP and SCA techniques, the nonconvex inequality constraint in (55b) can be approximated as the following convex inequality constraint, given by

$$\mathrm{tr}\left(\mathbf{R}_{\mathrm{D},k}\right) - 2\mathrm{Re}\left\{\left(\mathbf{f}_{\mathrm{D},k}^{(t)}\right)^H\mathbf{f}_{\mathrm{D},k}\right\} + \left(\mathbf{f}_{\mathrm{D},k}^{(t)}\right)^H\mathbf{f}_{\mathrm{D},k}^{(t)} \leq 0, \forall k, \tag{56}$$

where $\mathbf{f}_{\mathrm{D},k}^{(t)}$ is the solution obtained at the t-th iteration. Therefore, the convex approximation of problem (54) can be reformulated as

$$\min_{\mathbf{R}_{\mathrm{D},k},\mathbf{f}_{\mathrm{D},k},\mathbf{U}} \mathrm{tr}\left(\mathbf{D}\sum_{k=1}^{K}\mathbf{R}_{\mathrm{D},k}\right) - \sum_{k=1}^{K}2\mathrm{Re}\left\{\mathbf{f}_{\mathrm{D},k}^H\mathbf{e}_k\right\} \tag{57a}$$

$$\text{s.t.} \quad (52b), (52c), (54b), (54c), (54e), (55a), (56). \tag{57b}$$

Problem (57) is a convex problem, which can be solved by CVX.

Algorithm 2 Proposed SCA-BCD Algorithm for Solving Problem (24)

1: **Input:** Analog beamformer $\mathbf{F}_{\mathrm{A}}^{(0)}$, digital beamformer $\mathbf{F}_{\mathrm{D}}^{(0)}$, iteration index $n = 1$, and convergence tolerance δ.
2: **repeat**
3: Update $\boldsymbol{\gamma}^{(n)}$ by equation (43);
4: Update $\boldsymbol{\mu}^{(n)}$ by equation (44);
5: Update $\mathbf{F}_{\mathrm{A}}^{(n)}$ by solving problem (51);
6: Update $\mathbf{F}_{\mathrm{D}}^{(n)}$ by solving problem (57);
7: $n = n + 1$;
8: **until** The objective value of problem (24) is converged.
9: **Output:** $\mathbf{F}_{\mathrm{A}}$, $\mathbf{F}_{\mathrm{D}}$.

D. Overall Algorithm

The proposed SCA-BCD algorithm for solving the sensing SPEB-constrained communication sum-rate maximization problem (24) is summarized in **Algorithm** 2. The initial value of the nonzero elements of the analog beamformer is set to 1. The digital beamformer is first randomly initialized, and then is normalized to satisfy the transmit power constraint.

1) Convergence Analysis: The optimal solutions of $\boldsymbol{\gamma}$ and $\boldsymbol{\mu}$ are obtained based on the first-order optimality condition, and the locally optimal solutions of $\mathbf{F}_{\mathrm{A}}$ and $\mathbf{F}_{\mathrm{D}}$ are acquired by using SCA method. Hence, the objective value of problem (24) is monotonically nondecreasing [42]. Moreover, the sum-rate in problem (24) is upper-bounded due to the limited transmit power. Therefore, **Algorithm** 2 can be guaranteed to converge to a stationary point of problem (24).

2) Complexity Analysis: The computational complexity of **Algorithm** 2 is dominant by that of solving problem (51) and problem (57). Given a solution accuracy ϵ, the computational complexities for solving problem (51) and problem (57) are given by $\mathcal{O}\left(\log\left(1/\epsilon\right)N^{4.5}\right)$ and $\mathcal{O}\left(\log\left(1/\epsilon\right)K^{4.5}N_{\mathrm{RF}}^{4.5}\right)$, respectively. Thus, the total computational complexity of **Algorithm** 2 is given by $\mathcal{O}\left(N_{\mathrm{iter}}\log\left(1/\epsilon\right)\left(N^{4.5}+K^{4.5}N_{\mathrm{RF}}^{4.5}\right)\right)$, where N_{iter} denotes the number of iterations.

VI. Simulation Results

In this section, we provide numerical results to verify the effectiveness of the proposed HBF designs. We consider a near-field mmWave ISAC system operating at the carrier frequency of 28 GHz, where the BS equipped with $N = 32$ transmit and receive antennas simultaneously serves $K = 2$ single-antenna CUs and performs localization on one target. The aperture of the Tx/Rx arrays is $D = 0.5$ m, resulting in a Rayleigh distance of 46.7 m [18]. It is assumed that all the CUs and sensing target are located in the near-field region of the BS. Specifically, the CUs are randomly distributed on a semi-circle with the distance of 20 m away from the BS and the angle ranging from $-\pi/2$ to $\pi/2$, and the target is located at (10 m, 0). Unless otherwise specified, the simulation parameters are set in Table II.

For multiuser communication, the mmWave channel between the BS and each CU includes one LoS path and $L_k = 3$ NLoS paths. For each path, the angle of departure is randomly distributed in $[-\pi/2, \pi/2]$, the channel gain follows Gaussian distribution $\mathcal{CN}\left(0, 10^{-0.1\mathrm{PL}(d_k)}\right)$, where $d_k = \sqrt{x_k^2+y_k^2}$ represents the distance between the center of the Tx array and the k-th CU, and $\mathrm{PL}\left(d_k\right)$ is the distance-dependent path loss. Following the empirical NYC path loss model [43], the path loss of LoS and NLoS can be respectively computed as

$$\mathrm{PL}^{\mathrm{LoS}}\left(d_k\right)[\mathrm{dB}] = 61.4 + 20\log_{10}\left(d_k\right), \tag{58}$$

$$\mathrm{PL}^{\mathrm{NLoS}}\left(d_k\right)[\mathrm{dB}] = 72 + 29.2\log_{10}\left(d_k\right). \tag{59}$$

For target sensing, the reflection coefficient from the Tx to the Rx via the target can be expressed as

$$\beta = \sqrt{\frac{\lambda^2\sigma_{\mathrm{rcs}}}{(4\pi)^3 d_{\mathrm{s}}^4}}, \tag{60}$$

TABLE II
Simulation Parameters

Notation	Definition	Value
N	Number of antennas at the Tx/Rx	32
N_{RF}	Number of RF chains at the Tx	4
K	Number of CUs	2
f_c	Carrier frequency	28 GHz
λ	Signal wavelength	1.07 cm
D	Array aperture	0.5 m
$\frac{2D^2}{\lambda}$	Rayleigh distance	46.7 m
P	Transmit power of the BS	30 dBm
σ^2	Noise power	-90 dBm
$\mathrm{R}_{\min,k}$	Communication rate threshold	5 bps/Hz
Γ_s	Sensing SPEB threshold	0.04 m^2
T	Number of snapshots	100

where σ_{rcs} represents the RCS of the target, and $d_{\mathrm{s}} = \sqrt{x^2+y^2}$ represents the distance between the center of the Tx/Rx arrays and the target.

A. Communication Rate-Constrained SPEB Minimization

This subsection evaluates the performance of the proposed SDR-BCD algorithm for solving the communication rate-constrained SPEB minimization problem. Unless otherwise specified, the communication rate threshold is set as $\mathrm{R}_{\min,k} = 5$ bps/Hz, $\forall k$. The proposed beamforming designs and benchmark schemes are elaborated as follows:

- **Proposed SPEB-Min-based HBF:** The HBF is optimized to minimize the SPEB minimization under communication rate constraints by utilizing the proposed SDR-BCD algorithm.
- **Proposed SPEB-Min-based FDBF:** The FDBF is optimized to minimize the SPEB minimization under communication rate constraints by employing the SDR technique and eigenvalue decomposition.
- **SNR-Max-based HBF:** The HBF is optimized to maximize the sensing SNR under communication rate constraints [19].
- **Two-stage-based HBF:** In the first stage, the analog beamformer is optimized to maximize the beamforming gain towards the CUs and target, respectively. Specifically, the beams generated by K subarrays are focused on individual CUs, and the beams generated by the other $N_{\mathrm{RF}}-K$ subarrays are concentrated on the target. In the second stage, the digital beamformer is optimized by using the SDR technique to minimize the CRB for joint distance and angle estimation under communication rate constraints [18].

The localization accuracy of the above schemes are evaluated by the position error bound (PEB) [27], [28], which is defined as the square root of SPEB and is expressed as

$$\mathrm{PEB} = \sqrt{\mathrm{tr}\left(\left(\mathbf{J}_{\mathrm{e}}(x,y)\right)^{-1}\right)}. \tag{61}$$

Fig. 2 shows the convergence behaviour of the proposed SDR-BCD algorithm. We observe that the proposed SDR-BCD algorithm rapidly converges within a few iterations. As the number of RF chains increases, the convergence speed

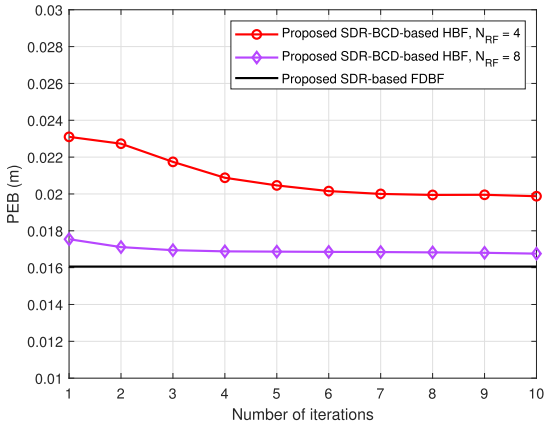

Fig. 2. Convergence of the proposed SDR-BCD algorithm.

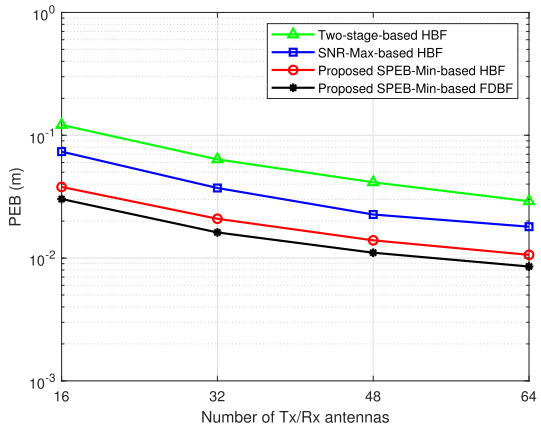

Fig. 4. Localization accuracy versus the number of Tx/Rx antennas.

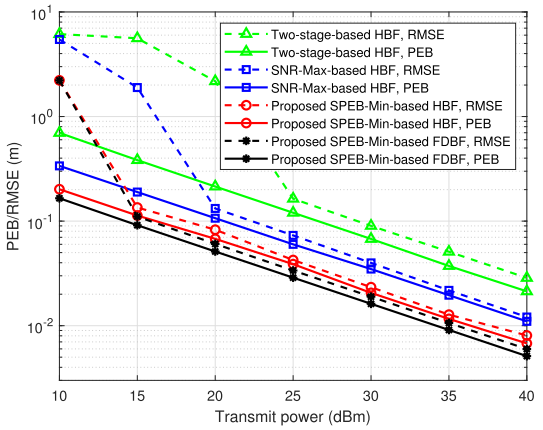

Fig. 3. Localization accuracy under various transmit powers.

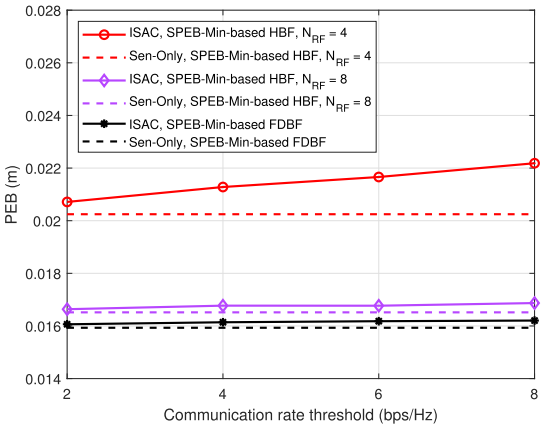

Fig. 5. Performance tradeoff between localization accuracy and communication rate.

becomes faster and the localization accuracy is improved due to the increased degrees of freedom.

Fig. 3 presents the target localization accuracy under various transmit powers. The root mean square error (RMSE) of target localization is obtained by the MUSIC algorithm. Specifically, the spatial spectrum is first constructed by projecting the far-field array response vector onto the noise subspace and the angle of target is estimated via one-dimensional (1D) search. Then, with the estimated angle, the distance of target is obtained via 1D search on the spatial spectrum constructed by the near-field array response vector. It is seen that the proposed SPEB minimization-based HBF can achieve localization accuracy close to the corresponding FDBF counterpart and outperform the existing two-stage-based HBF [18] and SNR maximization-based HBF [19], which demonstrates that adopting the SPEB minimization as the design criterion of beamforming can indeed improve the target localization accuracy compared to conventional approaches. When the transmit power is 30dBm, the RMSEs obtained by MUSIC-based near-field localization for the two-stage-based HBF, SNR maximization-based HBF, SPEB minimization-based HBF, and SPEB minimization-based FDBF are approximately 9cm, 4cm, 2.3cm, and 1.9cm, respectively. This indicates that the proposed algorithms are capable of achieving centimeter level localization accuracy. Moreover, the RMSE curves achieved by MUSIC-based localization are lower-bounded by the corresponding PEB curves in high SNR regimes, which verifies the correctness of our SPEB derivation and beamforming design.

Fig. 4 illustrates the impact of the number of antennas on localization accuracy. It is observed that the proposed SPEB minimization-based HBF can approach the FDBF counterpart and surpass the two-stage-based HBF [18] and SNR maximization-based HBF [19] in terms of localization accuracy. As the number of antennas increases, the localization accuracy of all the schemes can be improved. This is due to the fact that the increased antennas can provide larger beamforming gain for improving the received SNR, thereby enhancing the localization accuracy.

Fig. 5 investigates the performance tradeoff between localization accuracy and communication rate. We observe that the target localization accuracy of the proposed SPEB minimization-based ISAC FDBF and HBF deteriorates as the communication rate requirement of CUs increases. This is because the target localization and downlink multiuser communication share the identical transmit power resource. When the communication rate requirement improves, more power is allocated to the CUs, thereby resulting in the degradation of target localization accuracy. Moreover, the SPEB minimization-based sensing-only FDBF and HBF are presented as the theoretical performance bounds of the proposed

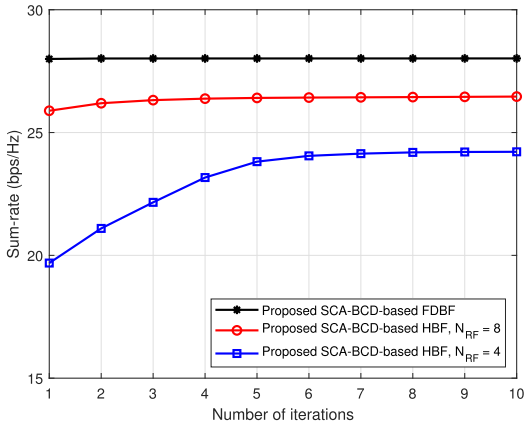

Fig. 6. Convergence of the proposed SCA-BCD algorithm.

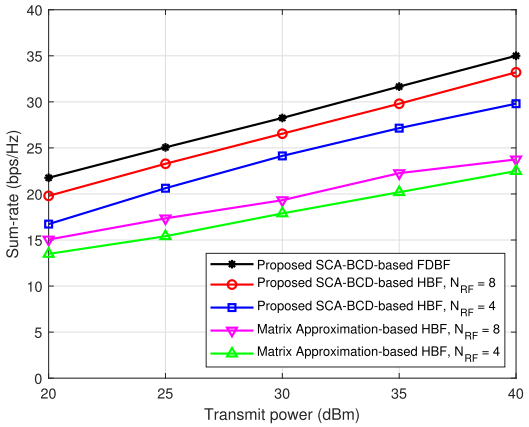

Fig. 7. Sum-rate under various transmit powers.

ISAC FDBF and HBF, respectively. As the number of RF chains increases, the PEBs achieved by the proposed ISAC FDBF and HBF are closer to the corresponding lower bounds given by the sensing-only FDBF and HBF, respectively, which validates the effectiveness of the proposed ISAC beamforming design.

B. Sensing SPEB-Constrained Sum-Rate Maximization

This subsection assesses the performance of the proposed SCA-BCD algorithm for solving the SPEB-constrained sum-rate maximization problem. Unless otherwise specified, the SPEB threshold of target localization is set as $\Gamma_s = 0.04$ m^2, i.e., the PEB threshold is $\sqrt{\Gamma}_s = 0.2$ m. The proposed algorithms and baseline schemes are described as follows:

- **Proposed SCA-BCD-based HBF:** The HBF is optimized to maximize the communication sum-rate under the sensing SPEB constraint by utilizing the proposed SCA-BCD algorithm.
- **Proposed SCA-BCD-based FDBF:** The FDBF can also be designed by applying the proposed SCA-BCD algorithm.
- **Matrix Approximation-based HBF:** As shown in [44], the analog beamformer and digital beamformer are alternately updated to approximate the fully-digital beamformer obtained by the **Proposed SCA-BCD-based FDBF**. However, this scheme theoretically cannot guarantee that the sensing SPEB constraint is always satisfied.

Fig. 6 depicts the convergence behaviour of the proposed SCA-BCD algorithm. As the number of iterations increases, the sum-rate of the proposed SCA-BCD algorithm monotonically increases and converges within several iterations. In addition, the convergence speed is improved as the number of RF chains increases.

Fig. 7 portrays the sum-rate under various transmit powers. We observe that the proposed SCA-BCD-based HBF can achieve performance close to the FDBF counterpart, especially when the number of RF chains is 8. In addition, the proposed SCA-BCD-based HBF significantly outperforms the conventional matrix approximation-based approach [44]. This is due to the fact that the matrix approximation-based HBF is tailored for single-user communication-only systems [44] and inevitably induces interuser interference in multiuser ISAC systems, thereby leading to significant sum-rate performance deterioration.

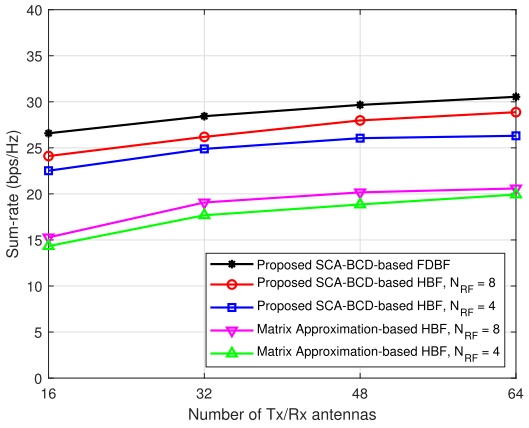

Fig. 8. Sum-rate versus the number of Tx/Rx antennas.

Fig. 8 presents the impact of the number of antennas on sum-rate. The proposed SCA-BCD-based HBF exhibits slight performance loss compared to the FDBF counterpart and achieves obvious performance gain compared to the existing matrix approximation-based HBF. As the number of antennas increases, the sum-rate of all the schemes can be improved due to the increased beamforming gain.

Fig. 9 depicts the tradeoff between communication sum-rate and target localization accuracy. As can be seen, the sum-rate achieved by the proposed SCA-BCD-based FDBF and HBF is improved as the sensing PEB threshold increases. In other words, the reduction in localization accuracy demand allows for the increase in power resource allocated to multiuser communication, thereby leading to the improvement of sum-rate. Furthermore, the FP-BCD-based communication-only FDBF and HBF are given as the theoretical performance upper bounds of the proposed SCA-BCD-based ISAC FDBF and HBF, respectively. When the number of RF chains is sufficiently large, the performance gap between the proposed ISAC beamforming design and the communication-only counterpart is negligible, which verifies the near-optimality of the proposed ISAC beamforming design.

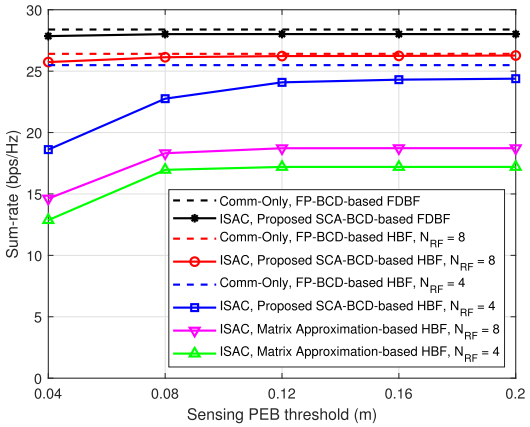

Fig. 9. Performance tradeoff between communication sum-rate and localization accuracy.

VII. Concultion

This paper investigated HBF design for near-field mmWave ISAC systems. The SPEB of near-field target localization was analyzed, based on which two HBF optimization problems were formulated to study the tradeoff between localization accuracy and communication rate. For the sensing-oriented HBF design, we proposed an SDR-BCD algorithm to solve the communication rate-constrained sensing SPEB minimization problem. For the communication-oriented HBF design, we proposed an SCA-BCD algorithm to address the sensing SPEB-constrained communication sum-rate maximization problem. Simulation results showed that the proposed SDR-BCD-based HBF can achieve localization accuracy close to the FDBF counterpart and surpass the benchmark schemes, and the proposed SCA-BCD-based HBF can achieve sum-rate similar to the corresponding FDBF and significantly outperform the existing schemes.

The single-target scenario was considered in this paper. In multi-target or large-scale user scenarios, how to design accurate near-field beamfocusing to achieve efficient interference management is a critical issue. Moreover, in high-mobility scenarios, the accurate acquisition of target position and velocity is challenging. It is of great significance to investigate the real-time trajectory tracking and robust beamforming in dynamic target scenarios [45], [46].

References

[1] F. Liu et al., "Integrated sensing and communications: Toward dual-functional wireless networks for 6G and beyond," *IEEE J. Sel. Areas Commun.*, vol. 40, no. 6, pp. 1728–1767, Jun. 2022.

[2] Y. Cui, F. Liu, X. Jing, and J. Mu, "Integrating sensing and communications for ubiquitous IoT: Applications, trends, and challenges," *IEEE Netw.*, vol. 35, no. 5, pp. 158–167, Sep. 2021.

[3] J. A. Zhang et al., "An overview of signal processing techniques for joint communication and radar sensing," *IEEE J. Sel. Topics Signal Process.*, vol. 15, no. 6, pp. 1295–1315, Nov. 2021.

[4] A. Liu et al., "A survey on fundamental limits of integrated sensing and communication," *IEEE Commun. Surveys Tuts.*, vol. 24, no. 2, pp. 994–1034, 2nd Quart., 2022.

[5] S. Lu et al., "Integrated sensing and communications: Recent advances and ten open challenges," *IEEE Internet Things J.*, vol. 11, no. 11, pp. 19094–19120, Jun. 2024.

[6] C. You et al., "Next generation advanced transceiver technologies for 6G and beyond," *IEEE J. Sel. Areas Commun.*, vol. 43, no. 3, pp. 582–627, Mar. 2025.

[7] M. Cui, Z. Wu, Y. Lu, X. Wei, and L. Dai, "Near-field MIMO communications for 6G: Fundamentals, challenges, potentials, and future directions," *IEEE Commun. Mag.*, vol. 61, no. 1, pp. 40–46, Jan. 2023.

[8] Y. Liu, Z. Wang, J. Xu, C. Ouyang, X. Mu, and R. Schober, "Near-field communications: A tutorial review," *IEEE Open J. Commun. Soc.*, vol. 4, pp. 1999–2049, 2023.

[9] Y. Liu, C. Ouyang, Z. Wang, J. Xu, X. Mu, and A. L. Swindlehurst, "Near-field communications: A comprehensive survey," *IEEE Commun. Surveys Tuts.*, vol. 27, no. 3, pp. 1687–1728, Jun. 2025.

[10] H. Zhang, N. Shlezinger, F. Guidi, D. Dardari, and Y. C. Eldar, "6G wireless communications: From far-field beam steering to near-field beam focusing," *IEEE Commun. Mag.*, vol. 61, no. 4, pp. 72–77, Apr. 2023.

[11] J. Cong et al., "Near-field integrated sensing and communication: Opportunities and challenges," *IEEE Wireless Commun.*, vol. 31, no. 6, pp. 162–169, Dec. 2024.

[12] Z. He et al., "Unlocking potentials of near-field propagation: ELAA-empowered integrated sensing and communication," *IEEE Commun. Mag.*, vol. 62, no. 9, pp. 82–89, Sep. 2024.

[13] M. Cui and L. Dai, "Channel estimation for extremely large-scale MIMO: Far-field or near-field?" *IEEE Trans. Commun.*, vol. 70, no. 4, pp. 2663–2677, Apr. 2022.

[14] Y. Lu, Z. Zhang, and L. Dai, "Hierarchical beam training for extremely large-scale MIMO: From far-field to near-field," *IEEE Trans. Commun.*, vol. 72, no. 4, pp. 2247–2259, Apr. 2024.

[15] H. Zhang, N. Shlezinger, F. Guidi, D. Dardari, M. F. Imani, and Y. C. Eldar, "Beam focusing for near-field multiuser MIMO communications," *IEEE Trans. Wireless Commun.*, vol. 21, no. 9, pp. 7476–7490, Sep. 2022.

[16] H. Wang, Z. Xiao, and Y. Zeng, "Cramér-Rao bounds for near-field sensing with extremely large-scale MIMO," *IEEE Trans. Signal Process.*, vol. 72, pp. 701–717, 2024.

[17] H. Hua, J. Xu, and Y. C. Eldar, "Near-field 3D localization via MIMO radar: Cramér-Rao bound analysis and estimator design," *IEEE Trans. Signal Process.*, vol. 72, pp. 3879–3895, 2024.

[18] Z. Wang, X. Mu, and Y. Liu, "Near-field integrated sensing and communications," *IEEE Commun. Lett.*, vol. 27, no. 8, pp. 2048–2052, Aug. 2023.

[19] K. Qu, S. Guo, N. Saeed, and J. Ye, "Near-field integrated sensing and communication: Performance analysis and beamforming design," *IEEE Open J. Commun. Soc.*, vol. 5, pp. 6353–6366, 2024.

[20] H. Li, Z. Wang, X. Mu, P. Zhiwen, and Y. Liu, "Near-field integrated sensing, positioning, and communication: A downlink and uplink framework," *IEEE J. Sel. Areas Commun.*, vol. 42, no. 9, pp. 2196–2212, Sep. 2024.

[21] F. Liu, Y.-F. Liu, A. Li, C. Masouros, and Y. C. Eldar, "Cramér-Rao bound optimization for joint radar-communication beamforming," *IEEE Trans. Signal Process.*, vol. 70, pp. 240–253, 2022.

[22] M. Yuan, H. Wang, H. Yin, and D. He, "Alternating optimization based hybrid transceiver designs for wideband millimeter-wave massive multiuser MIMO-OFDM systems," *IEEE Trans. Wireless Commun.*, vol. 22, no. 12, pp. 9201–9217, Dec. 2023.

[23] T. Yang et al., "A unified tensor-based joint AUD and ISAC parameter estimation with large-scale user access," *IEEE Trans. Cognit. Commun. Netw.*, early access, Feb. 25, 2025, doi: 10.1109/TCCN.2025.3545690.

[24] Q. Shi and M. Hong, "Penalty dual decomposition method for non-smooth nonconvex optimization—Part I: Algorithms and convergence analysis," *IEEE Trans. Signal Process.*, vol. 68, pp. 4108–4122, 2020.

[25] Y. Shen and M. Z. Win, "Fundamental limits of wideband localization—Part I: A general framework," *IEEE Trans. Inf. Theory*, vol. 56, no. 10, pp. 4956–4980, Oct. 2010.

[26] Y. Shen, H. Wymeersch, and M. Z. Win, "Fundamental limits of wideband localization—Part II: Cooperative networks," *IEEE Trans. Inf. Theory*, vol. 56, no. 10, pp. 4981–5000, Oct. 2010.

[27] A. Shahmansoori, G. E. Garcia, G. Destino, G. Seco-Granados, and H. Wymeersch, "Position and orientation estimation through millimeter-wave MIMO in 5G systems," *IEEE Trans. Wireless Commun.*, vol. 17, no. 3, pp. 1822–1835, Mar. 2018.

[28] Z. Abu-Shaban, X. Zhou, T. Abhayapala, G. Seco-Granados, and H. Wymeersch, "Error bounds for uplink and downlink 3D localization in 5G millimeter wave systems," *IEEE Trans. Wireless Commun.*, vol. 17, no. 8, pp. 4939–4954, Aug. 2018.

[29] G. Kwon, A. Conti, H. Park, and M. Z. Win, "Joint communication and localization in millimeter wave networks," *IEEE J. Sel. Topics Signal Process.*, vol. 15, no. 6, pp. 1439–1454, Nov. 2021.

[30] P. Gao, L. Lian, and J. Yu, "Cooperative ISAC with direct localization and rate-splitting multiple access communication: A Pareto optimization framework," *IEEE J. Sel. Areas Commun.*, vol. 41, no. 5, pp. 1496–1515, May 2023.
[31] X. Zhang, M. Peng, and C. Liu, "Sensing-assisted beamforming and trajectory design for UAV-enabled networks," *IEEE Trans. Veh. Technol.*, vol. 73, no. 3, pp. 3804–3819, Mar. 2024.
[32] N. González-Prelcic et al., "The integrated sensing and communication revolution for 6G: Vision, techniques, and applications," *Proc. IEEE*, vol. 112, no. 7, pp. 676–723, Jul. 2024.
[33] F. Liu and C. Masouros, "Hybrid beamforming with sub-arrayed MIMO radar: Enabling joint sensing and communication at mmWave band," in *Proc. IEEE Int. Conf. Acoust., Speech Signal Process. (ICASSP)*, May 2019, pp. 7770–7774.
[34] X. Wang, Z. Fei, J. A. Zhang, and J. Xu, "Partially-connected hybrid beamforming design for integrated sensing and communication systems," *IEEE Trans. Commun.*, vol. 70, no. 10, pp. 6648–6660, Oct. 2022.
[35] M. Yuan et al., "Hybrid beamforming for mmWave integrated sensing and communication with multi-static cooperative localization," *IEEE Trans. Wireless Commun.*, early access, Jul. 14, 2025, doi: 10.1109/TWC.2025.3586741.
[36] I. Bekkerman and J. Tabrikian, "Target detection and localization using MIMO radars and sonars," *IEEE Trans. Signal Process.*, vol. 54, no. 10, pp. 3873–3883, Oct. 2006.
[37] Z.-Q. Luo, W.-K. Ma, A. M.-C. So, Y. Ye, and S. Zhang, "Semidefinite relaxation of quadratic optimization problems," *IEEE Signal Process. Mag.*, vol. 27, no. 3, pp. 20–34, May 2010.
[38] Z. Wang, X. Mu, and Y. Liu, "STARS enabled integrated sensing and communications," *IEEE Trans. Wireless Commun.*, vol. 22, no. 10, pp. 6750–6765, Oct. 2023.
[39] K.-C. Toh, "An inexact primal–dual path following algorithm for convex quadratic SDP," *Math. Program.*, vol. 112, no. 1, pp. 221–254, Jul. 2007.
[40] K. Shen and W. Yu, "Fractional programming for communication systems—Part I: Power control and beamforming," *IEEE Trans. Signal Process.*, vol. 66, no. 10, pp. 2616–2630, May 2018.
[41] J. Zou, S. Sun, C. Masouros, Y. Cui, Y.-F. Liu, and D. W. K. Ng, "Energy-efficient beamforming design for integrated sensing and communications systems," *IEEE Trans. Commun.*, vol. 72, no. 6, pp. 3766–3782, Jun. 2024.
[42] M. Razaviyayn, M. Hong, and Z.-Q. Luo, "A unified convergence analysis of block successive minimization methods for nonsmooth optimization," *SIAM J. Optim.*, vol. 23, no. 2, pp. 1126–1153, Jan. 2013.
[43] M. R. Akdeniz et al., "Millimeter wave channel modeling and cellular capacity evaluation," *IEEE J. Sel. Areas Commun.*, vol. 32, no. 6, pp. 1164–1179, Jun. 2014.
[44] X. Yu, J.-C. Shen, J. Zhang, and K. B. Letaief, "Alternating minimization algorithms for hybrid precoding in millimeter wave MIMO systems," *IEEE J. Sel. Topics Signal Process.*, vol. 10, no. 3, pp. 485–500, Apr. 2016.
[45] J. Zhao, S. Xue, K. Cai, X. Mu, Y. Liu, and Y. Zhu, "Near-field integrated sensing and communications for secure UAV networks," 2025, *arXiv:2502.01003*.
[46] J. Wu, W. Yuan, and L. Bai, "On the interplay between sensing and communications for UAV trajectory design," *IEEE Internet Things J.*, vol. 10, no. 23, pp. 20383–20395, Dec. 2023.

Minghao Yuan received the B.S. degree in electronic information engineering from China University of Geosciences, Beijing, China, in 2018, and the M.S. degree in information and communication engineering from Beijing Institute of Technology, Beijing, in 2022, where he is currently pursuing the Ph.D. degree with the School of Information and Electronics. His current research interests include integrated sensing and communication (ISAC), extremely large-scale MIMO, and millimeter-wave communications.

Dongxuan He (Member, IEEE) received the B.S. degree in automation and the Ph.D. degree in information and communication systems from Beijing Institute of Technology (BIT) in 2013 and 2019, respectively. From 2017 to 2018, he was a Visiting Student at Singapore University of Technology and Design (SUTD). From 2019 to 2022, he was a Post-Doctoral Researcher at the Department of Electronic Engineering, Tsinghua University. He is currently an Assistant Professor at the School of Information and Electronics, BIT. His current research interests include integrated sensing and communication (ISAC), terahertz communications, and AI empowered wireless communications. He was a recipient of the Best Paper Award from the 2024 IEEE ICSIDP and the 2025 IEEE IWCMC. He is serving as a Guest Editor for IEEE OPEN JOURNAL OF THE COMMUNICATIONS SOCIETY, *Electronics*, and *Space: Science & Technology*. He was an Exemplary Reviewer of IEEE WIRELESS COMMUNICATIONS LETTERS.

Weijie Yuan (Senior Member, IEEE) is currently an Assistant Professor with the Southern University of Science and Technology. His research interests include integrated sensing and communications (ISAC), orthogonal time frequency space (OTFS), and the low-altitude wireless networks (LAWN). He is the Founding Chair of the IEEE ComSoc Special Interest Group (SIG) on LAWN as well as the SIG on OTFS. He was listed among the World's Top 2% Scientists by Stanford University for citation impact from 2021 to 2024, and among the Elsevier Highly-Cited Chinese Researchers. He was a recipient of the Best Editor from IEEE Communications Letters, the Best Paper Award from IEEE ICC 2023, IEEE/CIC ICCC 2023, and IEEE GlobeCom 2024, as well as the 2025 IEEE Communications Society and Information Theory Society Joint Paper Award. He serves as an Editor for IEEE TRANSACTIONS ON COMMUNICATIONS, IEEE TRANSACTIONS ON WIRELESS COMMUNICATIONS, IEEE TRANSACTIONS ON MOBILE COMPUTING, *IEEE Communications Magazine*, IEEE COMMUNICATIONS LETTERS, and IEEE OPEN JOURNAL OF COMMUNICATIONS SOCIETY; and a Guest Editor for IEEE TRANSACTIONS ON VEHICULAR TECHNOLOGY, IEEE TRANSACTIONS ON NETWORK SCIENCE AND ENGINEERING, and IEEE INTERNET OF THINGS JOURNAL.

Hao Yin received the B.S. degree in microwave communication and the M.S. degree in communication and information systems from Nanjing University of Posts and Telecommunications, Nanjing, China, in 1982 and 1987, respectively, and the Ph.D. degree in communication and information systems from Beijing Institute of Technology, Beijing, China, in 1999. He is currently an Adjunct Professor with the Army Engineering University of PLA, Nanjing, and a Researcher with Beijing Institute of Electronic System Engineering, Beijing. His research interests include wireless communication networks and information systems. He is a fellow of Chinese Academy of Sciences and China Institute of Communications.

Hua Wang (Member, IEEE) received the Ph.D. degree from Beijing Institute of Technology, Beijing, China, in 1999. From February 2009 to January 2010, he was a Visiting Professor with the Department of Electrical Engineering, Arizona State University, Tempe, AZ, USA. He is currently a Professor with the School of Information and Electronics, Beijing Institute of Technology. His research interests include communication theory and signal processing, wireless networking, and modem design and implementation for satellite communication.